Mechanical Systems and Signal Processing 205 (2023) 110867

Contents lists available at ScienceDirect

Mechanical Systems and Signal Processing

journal homepage: www.elsevier.com/locate/ymssp

Identification of cable tension through physical models and non-contact measurements

Cecilia Rinaldi [a,*], Marco Lepidi [b], Francesco Potenza [c], Vincenzo Gattulli [a]

[a] DISG - Department of Structural and Geotechnical Engineering, Sapienza University of Rome, Rome, Italy
[b] DICCA - Department of Civil, Chemical and Environmental Engineering, University of Genoa, Genoa, Italy
[c] INGEO - Department of Engineering and Geology, University "G. d'Annunzio" of Chieti-Pescara, Pescara, Italy

ARTICLE INFO

Communicated by F. Ubertini

Keywords:
Catenary cables
Perturbation methods
Inverse problem
Structural identification
Laser scanner
Cable-stayed bridge

ABSTRACT

Determining the static and dynamic response of structural cables is a mechanical problem of theoretical and practical interest in many aspects of civil engineering. In particular, the cable tension is a fundamental variable to be assigned in direct design problems, as well as a fundamental unknown to be assessed in inverse identification problems. The present paper outlines an original analytical strategy for identifying the axial tension of inclined sagged cables in cable-stayed structures, based on static measurements. Starting from the classic formulation of an inextensible, perfectly flexible model of catenary suspended cables, a perturbation-based low-order polynomial approximation of the static configuration under self-weight is achieved (*direct problem*). The quadratic and cubic coefficients of the configurational function are tension-dependent quantities, whose analytical expressions can be mathematically inverted to define consistent parametric formulas for tension identification (*inverse problem*). The experimental assessment of the static cable configuration, which serves as input for the inverse problem, is provided by the geometric data acquired by modern and noninvasive techniques of non-contact measurement. The methodological advantage is that the laser scanner acquisition of point cloud models can efficiently and economically provide precise and redundant three-dimensional geometric descriptions of the cable configuration, which is suitable for a highly accurate and statistically robust data treatment. Lastly, the identification strategy is successfully applied to a real-scale structure, for tension identification in the stays of a cable-stayed footbridge. The results are discussed from a qualitative and quantitative viewpoint, and finally validated through a comparison with the outcomes of a dynamic identification procedure based on high-speed camera acquisitions.

1. Introduction

Structural cables are considered among the most elegant, efficient and versatile solutions for resisting, carrying, or transmitting static and dynamic loads, with applications in a growing variety of traditional and emerging engineering fields. Over the past decades, cable structures have been studied by several theoretical and applied researchers, interested in investigating their rich and fascinating mechanical behavior, as well as in providing reliable recommendations for designers [1–5]. Specifically, the inherent combination of high material strength, shape-dependent geometric stiffness, low self-weight, aesthetic appeal and economic convenience makes cable nets – but also cable-beam, cable-arch and cable-ring collaborating structures – the ideal option for covering medium to large spans.

* Corresponding author.
E-mail address: cecilia.rinaldi@uniroma1.it (C. Rinaldi).

https://doi.org/10.1016/j.ymssp.2023.110867
Received 23 June 2023; Received in revised form 6 September 2023; Accepted 11 October 2023
Available online 25 October 2023

Within this framework, monitoring the health conditions of cable structures is a matter of considerable importance, not only because severe damages can determine collapses, but also because slight and moderate damages can significantly alter and/or early compromise the structural performance [6]. Moreover, because of their high flexibility and low inherent damping, structural cables are often exposed to important nonlinear dynamic phenomena, which have been widely studied in the literature through analytical and computational physical–mathematical models [2,7,8].

The current state-of-the-art in the field of non-destructive methods for structural health diagnosis of cables offer several physical indicators of damage, which can be classified either in the family of static and dynamic (mechanical) parameters, or in the complementary family of non-mechanical quantities [9,10]. The most common dynamic indicators can be determined using vibration-based techniques [11], and include natural frequencies, modal shapes, damping ratios, elastic dispersion properties, among the others. Non-mechanical indicators are determinable through multi-physical techniques, and vary from magnetic flux densities to optically reconstructed image patterns, from ultrasonic emission sources to ray reflection factors. Among the different mechanical indicators of cable damage, one of the most important variables is the axial internal force (or cable *tension*). Indeed, physical–mathematical models disclose that structural damages consisting of a reduction in the cable axial stiffness determine a tension loss and a sag increment in the static equilibrium configuration. This twofold peculiar mechanism causes a decrease in geometric stiffness (softening geometric effect), combined with an increase of the static curvature (hardening static effect), resulting in a systematic reduction of all linear frequencies and a modification of the symmetric modal shapes [12]. On the one hand, the marked tension-to-damage sensitivity in direct static and dynamic problems make the cable tension a suited detector for damage existence, location and severity (a combination of extent and intensity), according to identification procedures conceived as inverse modal problems and successfully verified through numerical simulations and experimental tests [13]. On the other hand, extensive technical applications tend to be slowed down by the evidence that cable tensions are also sensitive to different unavoidable mechanisms – such as softening or hardening effects due to thermal variations, small flexural stiffnesses and non-ideal boundary conditions –, which can either mask the damage (false negatives) or simulate non-existent damages (false positives). These considerations make the conception, development, and validation of reliable tension identification procedures an open issue of theoretical and practical interest and constitute the motivating background for further research studies.

From the methodological viewpoint, several techniques have been investigated in the recent decades to mechanically evaluate the in-service values of cable tension. Generally, they can be classified in direct and indirect methods. The former provide accurate and reliable results, but may require large energy consumption and specialized personnel to use expensive load-measuring instrumentation. The latter are based on the measurement of tension-dependent variables (strains, accelerations) and typically require easier and cost-effective nondestructive implementations, with lower but acceptable accuracy [14]. A second methodological classification categorizes mechanical methods for tension identification into static and dynamic techniques. Direct static methods rely on tension evaluation through a load cell or hydraulic jack, whereas indirect static methods require the statement of an inverse problem. In particular, the cable tension can be identified from displacement and strain differences between two static configurations (loaded and unloaded), by considering the length, stiffness, and mass per unit length of cable as unknowns [15]. Dynamic methods are instead indirect approaches that are generally targeted at identifying the cable tension by solving an inverse modal problem. Traditional dynamic techniques, typically based on the experimental knowledge of the lowest linear frequencies can provide high accuracy in the small-amplitude range of free oscillations [16]. However, the identification reliability depends not only on the uncertainties inherent to the measured data treatment, but also on the richness of the direct problem formulation. In this respect, comparative studies have highlighted the important role played by the sag-extensibility and flexural stiffness of cables [17].

From the analytical viewpoint, the simplest identification methods employ the taut-string theory, which completely neglects flexural stiffness and sag, thus returning convincing tension evaluations only for short stay cables anchored with simple supports. For long cables supported by complicated anchorage devices, combined methods including different experimental techniques are necessary [18]. As the real dynamic behavior of stay cables deviates from the linear relationship between the frequency and order of the corresponding mode, caused mainly by the flexural stiffness [19], several methods to correct the assumption of negligible flexural stiffness have been proposed [20,21]. As a major outcome, approximate modal solutions suited to propose practical identification formulas have been obtained for cables whose lowest frequencies are measurable, whereas formulas based on higher and antisymmetric vibration modes have been proposed for long cables, whose low-order modes are hardly excitable. Refined models have been developed by considering other mechanical effects, such as cable sag [22], sag and inclination angle [23], dampers attached in the proximity of the lower support [24,25], flexible supports [26]. From the computational viewpoint, system identification methods that consider both sag-extensibility and flexural stiffness have been proposed in the framework of finite element analyses, in combination with frequency-based sensitivity-updating algorithms [27]. More recently, similar updating procedures have been further developed by considering also the spatial variability of dynamic tension, unknown boundary conditions and lumped masses, with the aim of simultaneously identifying cable tension and other structural parameters [28,29].

Dynamic methods have the complementary advantage of being upgradable for real-time tension evaluation through real-time frequency identification [30,31]. Different methodologies have been proposed for this purpose, including an approach based on extended Kalman filters [32], an unsupervised learning algorithm (Complexity Pursuit) applied on a sliding short segment of two-channel accelerations [33], a novel adaptive sparse time–frequency analysis method (which combines Empirical Mode Decomposition method and Compressive Sensing theory) to accomplish the need for high resolution in the time–frequency domain and to reduce noise effects [34].

From the technological standpoint, non-contact techniques for data acquisition are becoming increasingly attractive for cable monitoring, because they are noninvasive and provide larger quantities of data with lower expenditure of human and instrumental

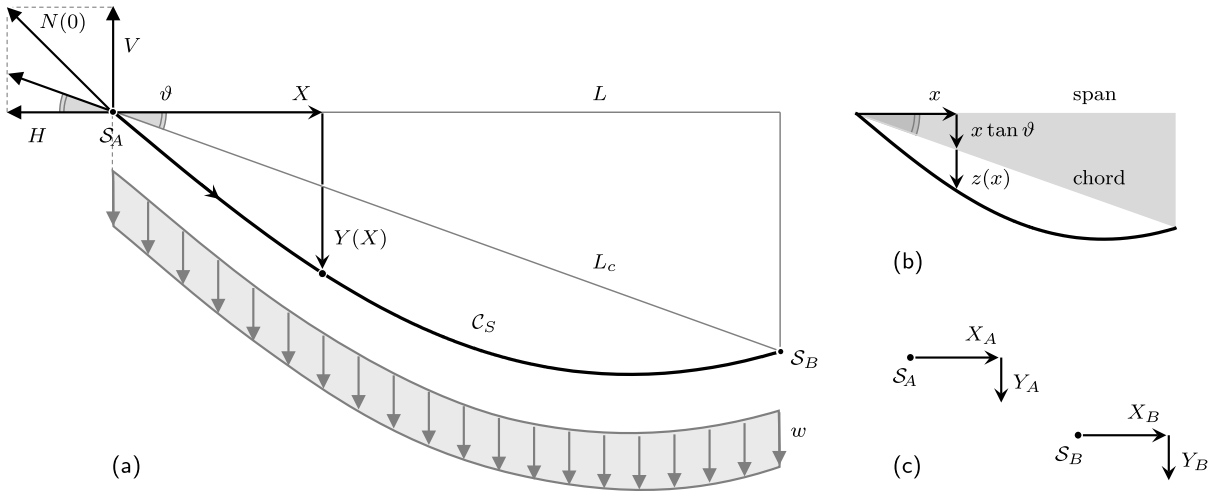

Fig. 1. Catenary cable suspended between fixed supports: (a) static equilibrium configuration $\mathcal{C}_S$ under self-weight, (b) nondimensional configuration functions, (c) support displacements.

resources. Among non-contact systems, laser vibration sensors [35,36], microwave remote sensing [37], acoustic radiation technology [38], and high-speed camera image processing [39,40] have proven to be very effective in recording cable vibrations for frequency-based tension identification. Such non-contact devices are mostly used for dynamic identification, whereas only a few investigations have been conducted on their use for static identification. Among a few others, a methodology based on static measurements has been proposed for assessing the force of short suspenders in suspension bridges [41]. Since the frequency-based method did not prove to be suitable, 3D laser scanning has been adopted to evaluate the point coordinates of the main cable intersection with suspenders and to implement an iterative convergence strategy for the inverse modeling of a finite element model, by considering the catenary equation for the equilibrium of the main cable under self-weight.

The key point emerging from the above discussion is that dynamic identification techniques are traditionally preferable because a few and easily measurable data (typically the lowest linear frequencies) suffice to provide an accurate and reliable assessment of the cable tension, according to the feasible mathematical inversion of more or less simplified direct modal problems. In contrast, static identification techniques are traditionally discarded, because the large amount of experimental data necessary to accurately describe the static problem solution (typically the static equilibrium configuration) is seldom available. Furthermore, the mathematical nature of the direct problem solution (catenary cable configuration under self weight) is rather unsuitable for analytical inversion. The primary objective of the present paper is to challenge this well-established scenario by (i) providing an analytical – although asymptotically approximate – and original solution for the inverse static problem relating the cable tension (unknown) to the catenary configuration (data), by employing a tailored perturbation method, and (ii) exploiting the powerful recent developments in the non-contact technology of laser scanning to achieve a largely accurate level of experimental knowledge for the cable configuration (high accuracy of data).

The paper is organized as follows. Section 2 describes the analytical formulation of the static equilibrium for suspended inclined cables, the perturbation solution of the direct problem, and its inverse formulation for tension identification. The case of stays in cable-stayed structures is also considered. Section 3 presents an overview of laser scanner technology and illustrates the particular strategy proposed to process the point cloud model, targeted at obtaining an accurate description of the cable configuration. Section 4 concerns with the application of the proposed tension identification method to a real-scale structure of interest in civil engineering. Specifically, the cable tensions in a cable-stayed footbridge are identified. The identification results are discussed and validated through direct comparison with a frequency-based dynamic method. Finally, the concluding remarks are presented.

2. Static equilibrium of the suspended cable

The static equilibrium of a suspended cable can be governed by formulating a monodimensional homogeneous continuous model. By adopting the ideal mechanical hypotheses of infinite axial rigidity and negligible shear and flexural rigidities, the cable model is assumed to be inextensible in the axial direction and perfectly flexible in the transversal directions. Owing to the inextensibility constraint and perfect transversal flexibility, the axial tension N must be intended as a reactive internal force, required to be locally collinear to the equilibrium configuration. Consequently, searching the cable response under gravity loads poses a geometric shape-finding problem, the solution of which consists in determining the unknown curvilinear configuration $\mathcal{C}_S$ that satisfies the equilibrium in the vertical plane (Fig. 1).

2.1. Problem formulation

The cable is supposed hanging between two fixed supports S_A and S_B, placed at different levels, under the sole effect of uniform self-weight w per unit length. For inclined cables characterized by the *inclination angle* ϑ, the *span* L, indicating the horizontal inter-support distance, differs from the *chord* $L_c = L\sec\vartheta$, indicating the inter-support distance. By selecting the horizontal abscissa $X \in [0, L]$ as independent variable, the configurational functions $Y(X)$ has to be determined to locate the Cartesian position of each cable point P in the vertical plane. The horizontal and vertical reactions H and V at the support S_A are also unknown.

Following a classic physical–mathematical formulation, the equilibrium equations governing the static response of inextensible cables can be derived by introducing the constraint of axial indeformability in the model of elastically deformable cables [1,5]. Specifically, the horizontal component of the axial tension $N(X)$ can be demonstrated to be constant and coincident with the reaction H, while the static equilibrium of the infinitesimal cable element is governed by the nonlinear ordinary differential equation

$$\frac{\mathrm{d}^2Y}{\mathrm{d}X^2} = -\frac{w}{H}\left[1 + \left(\frac{\mathrm{d}Y}{\mathrm{d}X}\right)^2\right]^{1/2} \tag{1}$$

which is also known as the *catenary equation*. The equation is fully characterized by the constant coefficient w/H affecting the right-hand term. The horizontal reaction H plays the role of hyperstatic unknown, to be determined a posteriori by imposing a geometric compatibility condition, according to a solution strategy resembling the force method. Particularly, the compatibility condition requires the cable inextensibility $L_e = L_0$, where L_0 is the natural length of the cable and L_e is the total arc-length of curved equilibrium configuration C_S. Naturally, an admissible solution can exist only if the natural length of the cable exceeds the inter-support chord length (mathematically, if the *admissibility condition* $L_0 > L_c$ is satisfied).

Solving analytically Eq. (1) for the boundary conditions $Y(0) = 0$ and $Y(L) = L\tan\vartheta$ returns a transcendental configurational function $Y(X)$, depending parametrically on the mechanical and geometrical data (w, L, ϑ, L_0). Geometrically, the solution describes the so-called *catenary* curve and also allows the analytical determination of the axial tension $N(X) = H\left[1 + \left(Y'(X)\right)^2\right]^{1/2}$ in the cable (*Direct problem*). Conversely, if some mechanical information is missing (L_0), the knowledge of the remaining data (w, L, ϑ), together with the experimental measure of the equilibrium configuration described by the function $Y(X)$ can be sufficient to identify the axial tension N in the cable (*Inverse problem* or *Identification problem*). Since the inversion of the direct problem may be mathematically challenging if the exact catenary solution is considered, an approximate – although asymptotically convergent – polynomial solution of the direct problem can be sought for, based on a suited perturbation approach.

2.2. Perturbation solution of the direct problem

Perturbation methods are powerful asymptotic techniques that are widely used in a large variety of scientific research fields, ranging from direct problems concerning linear and nonlinear dynamics, stability and bifurcation [42–45] to inverse problems dealing with modal identification, optimal spectral design, damping and damage detection [46–51]. Perturbation methods are also classical and well-established strategies to study different problems in cable mechanics, including static behaviors [52,53], linear and nonlinear dynamic phenomena [2,3,54–57], aerodynamic instabilities [58–60], active vibration control [61,62].

Due to their typical lightness (small w) and high tensioning (large H), structural cables tend to be characterized by geometric closeness (or *shallowness*) between the static equilibrium configuration and the inter-support chord. Consequently, the static problem for shallow cables can properly be reformulated by expressing the configuration function in the form $Y(X) = Y_c(X) + Z(X) = X\tan\vartheta + Z(X)$. The known function $Y_c(X) = X\tan\vartheta$ accounts for the vertical coordinate of the inter-support chord L_c, while the new configuration variable $Z(X)$ describes the *small* dip of the static configuration C_S below the chord (Fig. 1b). After the change of variable, Eq. (1) becomes

$$\frac{\mathrm{d}^2Z}{\mathrm{d}X^2} = -\frac{w}{H}\left[1 + \left(\tan\vartheta + \frac{\mathrm{d}Z}{\mathrm{d}X}\right)^2\right]^{1/2} \tag{2}$$

while the boundary conditions for fixed supports become homogeneous, reading $Z(0) = 0$ and $Z(L) = 0$.

Due to the smallness of the variable $Z(X)$, an asymptotic technique can profitably be adopted to pursue approximate solutions tending to the exact solution for increasing orders of a small nondimensional bookkeeping parameter. To this purpose, nondimensional quantities

$$x = \frac{X}{L}, \qquad z = \frac{Z}{L}, \qquad \Lambda = \frac{L_0}{L}\cos\vartheta, \qquad \delta = \frac{wL}{8H}, \tag{3}$$

where the parameter Λ, also known as *aspect ratio*, is the ratio between the natural length and the inter-support chord. The key parameter δ expresses instead the ratio between the approximate cable weight $wL\sec\vartheta$ and the approximate chord-aligned reaction $H\sec\vartheta$. By introducing nondimensional variables and parameters, the static equilibrium Eq. (2) reads in nondimensional form

$$\frac{\mathrm{d}^2z}{\mathrm{d}x^2} = -8\,\delta\left[1 + \left(\tan\vartheta + \frac{\mathrm{d}z}{\mathrm{d}x}\right)^2\right]^{1/2} \tag{4}$$

and the boundary conditions read $z(0) = 0$ and $z(1) = 0$. In this form, the role of hyperstatic unknown is played by the H-dependent parameter δ. The nondimensional compatibility condition reads $\Lambda_e = \Lambda$, where $\Lambda_e = (L_e/L)\cos\vartheta$, while the nondimensional compatibility condition reads $\Lambda > 1$.

Although unknown a priori, the parameter δ can certainly be considered small by hypothesis, as direct consequence of the assumption of cable shallowness. Therefore, a suited mono-parameter ordering is introduced by setting

$$\delta = \epsilon\delta_1 \tag{5}$$

where $\epsilon \ll 1$ is a nondimensional parameter with no physical meaning but a mere bookkeeping (scaling) role, regulating the smallness of the ϵ-ordered quantities. According to a standard perturbation strategy, the unknown variable $z(x)$ is postulated to be approximable by a finite series of n terms $z_i(x)$, scaled by increasing integer ϵ-powers

$$z_{[n]}(x) = \sum_{i=1}^{n} \epsilon^i z_i(x) = \epsilon\, z_1(x) + \epsilon^2 z_2(x) + ... + \epsilon^i z_i(x) + ... + \epsilon^n z_n(x) \tag{6}$$

where the functions $z_i(x)$ work as independent unknown variables. Once all the functions $z_i(x)$ are determined for $i = 1, \dots, n$, the approximate nth solution $z_{[n]}$ is expected to asymptotically tend to the exact solution for growing n-values (increasing *approximation orders*).

Substituting the parameter ordering (5) and the variable expansion (6) in the nonlinear Eq. (4), expanding and collecting terms of the same ϵ-power, an ordered hierarchical system of linear perturbation equations is obtained. Leaving aside the higher orders of the second (considering that the approximation order $n \leq 2$ is sufficient for the purposes of the present work), the system reads

$$\epsilon^1 : \qquad \frac{\mathrm{d}^2 z_1}{\mathrm{d}x^2} = -8\,\delta_1 \sec\vartheta, \tag{7}$$

$$\epsilon^2 : \qquad \frac{\mathrm{d}^2 z_2}{\mathrm{d}x^2} = -8\,\delta_1 \sin\vartheta \frac{\mathrm{d}z_1}{\mathrm{d}x}, \tag{8}$$

while homogeneous boundary conditions $z_i(0) = 0$ and $z_i(1) = 0$ must be imposed at each order.

The system solutions can be obtained straightforwardly by attacking the linear equations in cascade, starting from the uncoupled lowest order (7), returning the *generating solution* $z_1(x)$. Thereafter, the second order (8) states an ordinary differential non-homogeneous equation involving only the second derivative of the unknown variables $z_2(x)$, at the left hand, and the known derivatives of the generating solution $z_1(x)$, at the right hand. The solutions are polynomial functions reading

$$\epsilon^1 : \qquad z_1(x) = 4\,\delta_1 \sec\vartheta\, x(1-x) \tag{9}$$

$$\epsilon^2 : \qquad z_2(x) = \tfrac{16}{3}\delta_1^2 \tan\vartheta\, x(1-x)(1-2x), \tag{10}$$

where $z_1(x)$ and $z_2(x)$ can be recognized to be a quadratic x-function, affected by multiplier δ_1, and a cubic x-function, affected by multiplier δ_1^2, respectively. Furthermore, $z_1(x)$ and $z_2(x)$ can be recognized to be a symmetric and an antisymmetric function with respect to the *midspan* ($x = 1/2$).

Therefore, the asymptotic solution can be reconstructed by substituting the perturbation solutions (9) and (10) in the series (6), taking care about properly inverting the ordering relation (5) to completely reabsorb the parameter ϵ. The reconstructed solution reads

$$z_{[2]}(x) = 4\,\delta \sec\vartheta \left(1 + \tfrac{4}{3}\delta \sin\vartheta\right) x - 4\,\delta \sec\vartheta\,(1 + 4\delta \sin\vartheta)\, x^2 + \tfrac{32}{3}\delta^2 \tan\vartheta\, x^3 \tag{11}$$

that is a cubic function, in which the second-order antisymmetric contribution $z_2(x)$ perturbs the symmetry of the first order contribution $z_1(x)$. From the mathematical viewpoint, the reconstructed solution $z_{[2]}(x)$ is expected to approximate the exact solution with difference belonging to the order $\mathcal{O}(\epsilon^3)$, or $\mathcal{O}(\delta^3)$ after reabsorption. From the mechanical viewpoint, an intuitive physical interpretation of the smallness $\mathcal{O}(\delta^3)$ can be given by noting that the lowest-order approximation of the cable *sag* (dip at midspan) is $z_1(1/2) = \delta \sec\vartheta$. Such crucial result discloses an alternative physical interpretation of the key parameter δ, which actually expresses the *sag-to-span ratio* of the parabolic cable characterized by a certain aspect ratio Λ, suspended between leveled supports (for inclination angle $\vartheta = 0$).

The hyperstatic unknown δ remains to be determined by imposing the compatibility condition $\Lambda_e = \Lambda$. According to differential geometry, the nondimensional arc-length Λ_e has the integral expression

$$\Lambda_e = \cos\vartheta \int_0^1 \left[1 + \left(\tan\vartheta + \frac{\mathrm{d}z}{\mathrm{d}x}\right)^2\right]^{1/2} \mathrm{d}x \tag{12}$$

which can be asymptotically approximated by operating accordingly to the perturbation scheme ruled by Eqs. (5) and (6). Specifically, the perturbation-based solution of the integral returns the second-order approximation

$$\Lambda_{[2]} = 1 + \frac{8}{3}\delta^2 \cos^2\vartheta \tag{13}$$

which is expected to approximate the exact length Λ_e with difference of order $\mathcal{O}(\delta^4)$, which is fully consistent with the approximation order of the solution $z_{[2]}(x)$.

To summarize, approaching the direct problem requires (i) to assign the chord inclination ϑ and cable aspect ratio Λ, which are the only free nondimensional parameters, and (ii) to solve the compatibility equation $\Lambda_{[2]} = \Lambda$ in the hyperstatic unknown δ. The inclination angle must be chosen in the range $0 \leq \vartheta < \pi/2$. The aspect ratio must be assigned without violating the admissibility

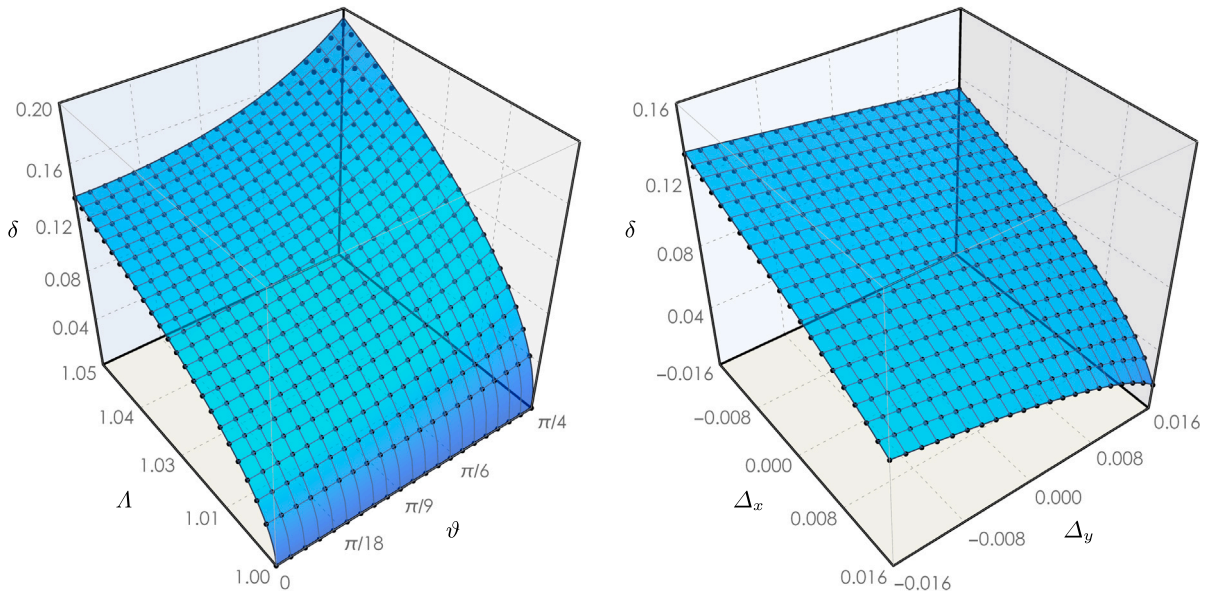

Fig. 2. Exact hyperstatic unknown δ (black dots) compared with its asymptotic approximation $\delta_{[2]}$ (blue surface): (a) fixed supports and varying mechanical parameters in the relevant range of aspect ratios $\Lambda \in [100/100, 105/100]$ and inclination angles $\vartheta \in [0, \pi/4]$, (b) fixed mechanical parameters ($\Lambda = 102/100$, $\vartheta = \pi/8$) and displaceable supports in the admissible ranges $\Delta_x \in [-16/1000, 16/1000]$ and $\Delta_y \in [-16/1000, 16/1000]$.

condition $\Lambda > 1$ and respecting the requirement of shallowness $\Lambda - 1 = \mathcal{O}(\delta^2)$ that follows from Eq. (13). Therefore, the hyperstatic unknown can be determined as

$$\delta_{[2]} = \left(\frac{3}{8} \frac{(\Lambda - 1)}{\cos^2 \vartheta} \right)^{1/2} \tag{14}$$

where it can be noted that the condition $\Lambda > 1$ systematically suffices to ensure real-valued solutions. In this respect, it can be remarked that the null value $\delta_{[2]} = 0$ (no sag) is recovered for the limit case $\Lambda \to 1$ (natural length equal to the chord), as expected for inextensible cables.

A parametric analysis carried out to compare the exact hyperstatic unknown δ with its asymptotic approximation $\delta_{[2]}$ is illustrated in Fig. 2. The effective accuracy of the approximation in the relevant range of aspect ratios Λ and inclination angles ϑ is qualitatively certified by the closeness between the loci of δ-values (numerically determinable and marked by black dots) and $\delta_{[2]}$ (analytically evaluated and described by the blue surface). From the quantitative viewpoint, the asymptotic approximation $\delta_{[2]}$ can be recognized to slightly overestimate the exact solution δ for large aspect ratios and high inclination angles. Nonetheless, the relative difference $(\delta_{[2]} - \delta)/\delta$ is systematically lower than 0.03 in all the (Λ, ϑ)-parameter space, apart in the limit region where $\Lambda \to 1$ and $\delta \to 0$.

Once hyperstatic unknown $\delta_{[2]}$ is known, the reconstructed solution $z_{[2]}(x)$ is determined and can be employed in the inverse change of coordinate necessary to assess the second-order approximation of the cable configuration function

$$y_{[2]}(x) = \tan \vartheta \, x + \gamma_2 x + \gamma_1 x^2 + \gamma_0 x^3 \tag{15}$$

where the first term describes the vertical coordinate of the cable chord and can be recognized to belong to $\mathcal{O}(\delta^0)$, consistently with the perturbation approach. The independent configurational coefficients of the other terms read

$$\gamma_0 = \tfrac{32}{3} \delta_{[2]}^2 \tan \vartheta \qquad \gamma_1 = -4 \, \delta_{[2]} \sec \vartheta \left(1 + 4 \delta_{[2]} \sin \vartheta \right) \tag{16}$$

whereas the last configurational coefficient γ_2 is dependent on the others according to the relation $\gamma_2 = -(\gamma_0 + \gamma_1)$. It is worth noting that $\gamma_0 > 0$ and $\gamma_1 < 0$, by definition.

Finally, the nondimensional axial tension $\nu = N/H$ is an x-dependent function that can be determined by leveraging the nondimensional relation

$$\nu(x) = \left[1 + \left(\frac{\mathrm{d}y}{\mathrm{d}x} \right)^2 \right]^{1/2} \tag{17}$$

which, consistently with the other variables, can be asymptotically approximated accordingly to the same perturbation scheme. Skipping all the technical details, its second-order approximation reads

$$\nu_{[2]}(x) = \sec \vartheta + 4 \delta_{[2]} \tan \vartheta (1 - 2x) + \tfrac{8}{3} \delta_{[2]}^2 \sec \vartheta \left[2 - 12 \, x(1 - x) + \cos^2 \vartheta \right] \tag{18}$$

which is expected to approximate the exact length Λ_e with difference belonging to the order $\mathcal{O}(\delta^3)$, which is fully consistent with the approximation order of the solution $z_{[2]}(x)$.

2.3. Inverse problem for tension identification

In the inversion of direct mechanical problems, the data and unknowns typically exchange their respective roles. More precisely, a certain discretion may exists in selecting the data actually available (typically a measurable subset of all the possible data), as well as in choosing one or more preferred unknowns to be primarily identified (among all the missing information). Therefore, direct and inverse problems may share part of the data and/or part of the unknowns.

Focusing on the particular system under investigation and starting from the data, some geometric and mechanical information of the direct problem are considered known also for the inverse problem. Specifically, the uniform weight per unit length w, the span L and the inclination angle ϑ of the cable are assumed known. This assumption does not contradict the spirit of the present work, because – even if they were unknown a priori – all these quantities would be actually measurable by means of merely static or geometric procedures. It is worth noting that the natural cable length L_0 (or equivalently the aspect ratio Λ) is not assumed known.

Turning to the unknowns, the direct problem returns the equilibrium configuration of the cable, as primary result described by the configurational function $Y(X)$, and the cable tension $N(X)$, as complementary result. Differently, the inverse problem adopts the nondimensional function $y(x)$ as known information, while the cable tension $N(X)$ remains as primary unknown to be determined. Specifically, if shallow cables are considered, the equilibrium configuration can be described with sufficient accuracy by the nondimensional cubic approximation $y_{[2]}(x)$, so that the configurational data reduce to the pair of independent coefficients γ_0 and γ_1. In this respect, the experimental assessment of the coefficients is a technical matter of data treatment for geometric restitution, which is methodologically detailed in the next Section.

Once the two configurational coefficients are experimentally assessed, determining the cable tension is an overdetermined problem, featuring two data (γ_0 and γ_1) and one unknown (the tension $N(x)$, or equivalently its horizontal component H). Instead of recurring to classical solution schemes (like, for instance, the method of least squares), it may be convenient to recall that – according to the perturbation scheme – the quadratic coefficient γ_1 (being $\mathcal{O}(\delta)$) is larger than the cubic coefficient γ_0 (being $\mathcal{O}(\delta^2)$). Therefore, it can be expected that the quadratic coefficient γ_1 might be experimentally assessed with higher precision, and thus could be preferred for the analytical identification of the horizontal tension. Accordingly, if the coefficient γ_1 is known, the second of the Eqs. (16) states a quadratic algebraic equation in the unknown nondimensional sag-to-span ratio δ. Once the algebraic equation is solved, the last of parametric relations (3) can be inverted to identify the horizontal reaction according to the formula

$$\hat{H} = \frac{wL}{8\hat{\delta}} = -\frac{1+\sqrt{1-2\hat{\gamma}_1 \sin(2\vartheta)}}{4\hat{\gamma}_1 \cos\vartheta} wL \tag{19}$$

where the overhat indicates directly measured quantities, or quantities identified from measures. It is worth remarking that the formula (19) returns positive tensions $\hat{H} > 0$, since $\hat{\gamma}_1 < 0$ and $0 \le \vartheta < \pi/2$. Therefore, the cubic coefficient $\hat{\gamma}_0$ can profitably be employed to evaluate the quality of the identification by checking the smallness of the quantity

$$\hat{e} = \frac{wL}{\hat{H}} \sqrt{\frac{\tan\vartheta}{6\hat{\gamma}_0}} - 1 \tag{20}$$

which expresses the relative difference between the γ_0-based and γ_1-based identification. As a major remark, the tension identification does not require the knowledge of the aspect ratio $\Lambda = (L_0/L)\cos\vartheta$, that is, the natural length L_0 of the cable is not an information required in the inverse problem. Although counter-intuitive, this advantageous point is mechanically justified by considering that the aspect ratio influences only the hyperstatic unknown δ (see Eq. (14)). The hyperstatic unknown, however, influences only the coefficients γ_0 and γ_1 (see Eq. (16)), which – in the inverse problem – are not calculated but experimentally assessed. As a minor remark, the identification formulas (19) and (20) can be expressed in fully dimensional form by replacing $\hat{\gamma}_1 \to \hat{k}_1 L$ and $\hat{\gamma}_0 \to \hat{k}_0 L^2$, where $\hat{k}_1$ and $\hat{k}_0$ are the identifiable coefficients of the dimensional cubic configuration $Y_{[2]}(X) = \tan\vartheta X + k_2 X + k_1 X^2 + k_0 X^3$.

Finally, the variable axial tension $N(x)$ can be determined by employing the dimensional form of Eq. (17). By conveniently adopting the second order approximation (18), the axial tension can be approximated as $N_{[2]}(X) = H v_{[2]}(X/L)$ in the direct problem. Consistently, in the inverse problem it can be identified according to the formula

$$\hat{N}(X) = \hat{H}\sec\vartheta + \frac{wL\tan\vartheta}{2} + \frac{w^2L^2(2+\cos^2\vartheta)}{24\hat{H}\cos\vartheta} - \frac{w(wL+2\hat{H}\sin\vartheta)X}{2\hat{H}\cos\vartheta} + \frac{w^2X^2}{2\hat{H}\cos\vartheta} \tag{21}$$

where a constant and a x-dependent part can be recognized. The minimal approximation formula $\hat{N} \simeq \hat{H}\sec\vartheta$ can be extracted, by retaining only the lowest-order term.

2.4. Tension identification in cable stayed structures

Cables are mostly employed as sustaining or stiffening elements in geometrically complex and highly hyperstatic engineering structures, composed by several three-dimensional interconnections of different structural members (cables, beams, arches, plates). Consequently, extending the static strategy for tension identification to cable-stayed structures can be a matter of theoretical and applied interest.

According to the direct stiffness method and without loss of generality, the other structural members can be considered to interact with a stay cable through static nodal loads exerted at the cable ends. Therefore, it is possible to demonstrate *analytically* that the solution of the inverse problem can be expressed independently of the nodal loads, provided that the data of the inverse problem

account for the nodal displacements of the cable ends. Briefly, the demonstration can be based on: (i) extending the asymptotic solution of the direct problem in order to parametrically include the effects of generic nodal displacements at the cable ends, (ii) proving mathematically that the analytical inversion of the extended solution provides an identification formula for the cable tension that can be systematically reduced to the formula obtained for fixed supports, (iii) recalling the assumptions of the inverse problem, according to with the static configuration of the cable (including nodal displacements) is completely known from experimental measurements.

First, the direct problem can be reformulated by relaxing the assumption of fixed supports. Consequently the horizontal and vertical displacements at the supports S_A and S_B can be described by the nondimensional quantities $x_A = X_A/L, y_A = Y_A/L$ and $x_B = X_B/L, y_B = Y_B/L$ (Fig. 1c). The static configuration function of the inextensible cable suspended between displaceable supports can be expressed in the form $y_d(x) = y_d(x) + z_d(x) = a_1 + a_0 x + z_d(x)$. The known function $y_d(x) = a_1 + a_0 x$, with coefficients $a_0 = \left(y_B - y_A + \tan\vartheta\right)/\left(1 - x_A + x_B\right)$ and $a_1 = \left[y_A(1 + x_B) - x_A(y_B + \tan\vartheta)\right]/\left(1 - x_A + x_B\right)$ describes the vertical coordinate of the chord between the displaced supports. By following an asymptotic strategy similar to the perturbation method described in Section 2.2, the new configuration variable $z_d(x)$ can be asymptotically approximated in polynomial series (algorithmic details are reported in [63]). Considering terms up to the second order, the reconstructed configuration function has the cubic form

$$y_{d[2]}(x) = a_1 + a_0 x + z_{[2]}(x) = a_1 + a_0 x + \beta_2 x + \beta_1 x^2 + \beta_0 x^3 \tag{22}$$

where the high-order coefficients reads

$$\beta_0 = \tfrac{32}{3} a_0 \delta_{[2]}^2, \qquad \beta_1 = -4\delta_{[2]}(c_0 + 4a_0\delta_{[2]}(1 + x_A + x_B)), \qquad \beta_2 = \tfrac{4}{3}\delta_{[2]}\left(3c_0(1 + x_A + x_B) + 4a_0\delta_{[2]}Q_x\right), \tag{23}$$

where the auxiliary quantities $Q_x = x_A^2 + 4x_A(1 + x_B) + (1 + x_B)^2$ and $c_0^2 = 1 + a_0^2$ have been introduced. By imposing the compatibility condition of cable inextensibility, the hyperstatic unknown $\delta_{[2]}$ can be determined analytically as an explicit function of the support displacement differences $\Delta_x = x_B - x_A$ and $\Delta_y = y_B - y_A$ [63]. This dependence is illustrated in Fig. 2b.

Second, a couple of auxiliary nondimensional parameters $\tilde{\Lambda} = \tilde{L}/L$ and $\tilde{\vartheta} = \arctan \tilde{B}/\tilde{L}$ can be introduced, where $\tilde{L} = L - X_A + X_B$ and $\tilde{B} = L\tan\vartheta - Y_A + Y_B$. By virtue of these definitions, a proper change of coordinates $x \to \tilde{x} + x_A$, $y \to \tilde{y} + y_A$ and a few appropriate reparameterizations $\tan\vartheta \to y_A - y_B + (1 - x_A + x_B)\tan\tilde{\vartheta}$, $\delta \to \tilde{\delta}/\tilde{\Lambda}$, $x_B \to \tilde{\Lambda} - 1 + x_A$ allow to express the configuration function (22) in the form

$$\tilde{y}_{[2]}(\tilde{x}) = \tan\tilde{\vartheta}\tilde{x} + \tilde{z}_{[2]}(\tilde{x}) = \tan\tilde{\vartheta}\tilde{x} + \tilde{\beta}_2\tilde{x} + \tilde{\beta}_1\tilde{x}^2 + \tilde{\beta}_0\tilde{x}^3 \tag{24}$$

where the independent quadratic and cubic coefficients read

$$\tilde{\beta}_0 = \tfrac{32}{3}\tilde{\delta}^2\tan\tilde{\vartheta}, \qquad \tilde{\beta}_1 = -4\,\tilde{\delta}\sec\tilde{\vartheta}\left(1 + 4\tilde{\delta}\sin\tilde{\vartheta}\right) \tag{25}$$

while the linear coefficient $\tilde{\beta}_2 = -\left(\tilde{\beta}_0 + \tilde{\beta}_1\right)$. It is fundamental to remark that the configuration function (24) is formally analogous to the configuration function (15) for fixed supports, except for the redefinition of the variables and parameters. Noteworthy, in the new space of variables and parameters the coefficients do not explicitly depend on the support displacements.

Finally, by exploiting the mathematical analogies between the configuration functions (15) and (24) and recalling the relation $\delta = \tilde{\delta}/\tilde{\Lambda}$, the identification formula for the horizontal tension in the cable suspended between supports undergoing generic displacements reads

$$H = \frac{wL}{8\tilde{\delta}}\tilde{\Lambda} = -\frac{1 + \sqrt{1 - 2\tilde{\beta}_1\sin(2\tilde{\vartheta})}}{4\tilde{\beta}_1\cos\tilde{\vartheta}}w\tilde{L} \tag{26}$$

where, remarkably, the knowledge of the support displacements is unnecessary. Differently, the minimal necessary information consists of the parameter set $\tilde{L}$, $\tilde{\vartheta}$, $\tilde{\beta}_1$. According to the reparameterizations, they can be recognized as the cable span $\tilde{L}$, the inclination angle $\tilde{\vartheta}$ and the nondimensional quadratic coefficient $\tilde{\beta}_1$. By definition, they pertain to the cubic configuration attained by the cable under self weight *and* support displacements and, by hypothesis of the inverse problem, are known (measurable) quantities.

To exemplify, the tension identification strategy is applied to the inclined stay supporting the *cable-stayed beam* (Fig. 3), which is a widely recognized paradigmatic system for studying the static and dynamic collaboration between beams and cables in complex cable structures [64,65]. The solution of the static problem for Euler–Bernoulli beam (with axial stiffness EA, flexural stiffness EI, self-weight w_b) and inclined catenary or cubic inextensible cable (with span L, inclination angle ϑ, aspect ratio Λ and self-weight w) can be determined exactly [66]. Considering the cubic cable, the exact solution can synthetically be described by a minimal set of significant unknowns, including the horizontal tension H, the displacements $U = X_B$ and $V = -Y_B$ at the cable-beam node, and the quadratic coefficient $k_1 = \beta_1 L$. Assigned certain mechanical parameters as data for the direct problem, the values obtained for this unknowns are reported in Table 1. Therefore, by deterministically adopting these exact results as noise-free pseudo-experimental data for the inverse problem (which implies calculating the (U, V)-dependent reparameterizations $\tilde{L}, \tilde{\vartheta}$ and $\tilde{k}_1 = \tilde{\beta}_1\tilde{L}$ that are actually measured in real experimental applications), the cable tension H can be verified to be successfully identified without errors by employing the formula (26).

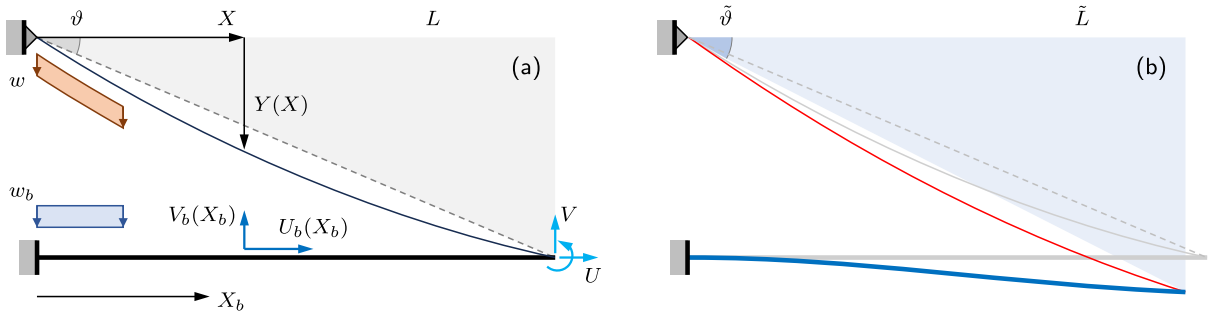

Fig. 3. Cable-stayed beam: (a) reference configuration (cable with fixed supports), (b) static equilibrium configuration.

Table 1
Solutions of the direct and inverse static problem for the cable stayed beam (with assigned mechanical parameters $L = 10$, $\vartheta = \pi/8$, $\Lambda = 1005/1000$, $w = 1/10000$, $EA = 10000$, $EI = 1000$, $w_b = 1/20$).

Unknown	H	U	V	k_1	$\tilde{L}$	$\tilde{\vartheta}$	$\tilde{k}_1$
Result	0.00356772	−0.0000036	−0.06217854	−0.01602858	9.99999643	0.39799479	−0.01615834

3. Geometric reconstruction of the cable configuration

The inverse problem for tension identification considers the cable tension as primary unknown and the geometric static configuration as known information, as discussed in the previous Section. The geometric configuration can be determined experimentally by non-contact measurement devices, such as cameras and scanners, and returned as a three dimensional point cloud model (*Phase 1 – Point cloud acquisition*). Such kind of experimental data needs to be post-processed to achieve a geometric description of the cable configuration that is coherent with the analytical formulation of the inverse identification problem (*Phase 2 – Cubic configuration from data*). Therefore, this section aims at, first, briefly reporting a general overview about three-dimensional point cloud acquisitions with the available laser scanning technologies and, second, describing the particular post-processing data treatment proposed to achieve the coherent geometric reconstruction of the cable configuration. For the sake of comparison, a short description of the alternative image-based technologies of vibration measurement that will be used in the following to validate the identification results is reported in Appendix.

3.1. Laser scanning point cloud acquisition

Point cloud models are discrete sets of data points describing the geometry of an object or volume. Three-dimensional models can be generated by using technologies that exploit images from camera or data from different non-contact scanner categories [67]. Both these tools allow a non-contact acquisition of the geometry data, but scanning technology is less time-consuming, is rather independent of light conditions and also does not require additional data processing to extract coordinate information from images [68]. Among other available technologies, the scanning process based on optical reflections of laser signals is encountering increasing success for structural health monitoring applications. The three-dimensional geometric reconstruction of structures is obtained by sending exploring laser beams consisting of electromagnetic signals propagating in the optical wavelength range, namely photonic waves or photons. The wave signals can be reflected by the target surface of the scanned object. Some of reflected signals come back to the photosensitive sensor of the scanner. The inter-distance between the device and reflecting points of the object surface can be evaluated and, depending on the distance evaluation method, laser scanners can be classified into different categories [67]. Specifically, *triangulation scanners* trigonometrically determine the triangle formed by the camera, the transmitter that sends the laser beam, and the spot of the laser beam (intersection of the beam with the object). *Time-of-flight systems*, also called pulse measurement systems, measure the time taken by the laser beam (propagating with known velocity) to be reflected back to the photosensitive sensor. Differently, *phase-shift systems*, which emit continuous laser beams, measure the phase shift between the sent and the received signals. Finally, *structured light scanners* are based on the projection of a pattern; by using a camera, the analysis of pattern deformations caused by the object shape allows to reconstruct the three-dimensional position of several points at once.

3.2. Cubic configuration from point cloud

The geometric curved profile assumed by a suspended cable hanging on a vertical plane under self-weight is supposed to be described by the dataset $\mathcal{P}$ (*cloud model*) of n_C laser-scanned points. The generic ith point $P_i \in \mathcal{P}$ is pointed by the position vector $\mathbf{X}_i = (X_i, Y_i, Z_i)$, within an Cartesian reference system of orthogonal coordinates in a three-dimensional space (with $i = 1, \dots, n_C$). The origin point is located at the laser source. The vertical mid-plane of the point cloud (Fig. 4) is fully defined by its intersection

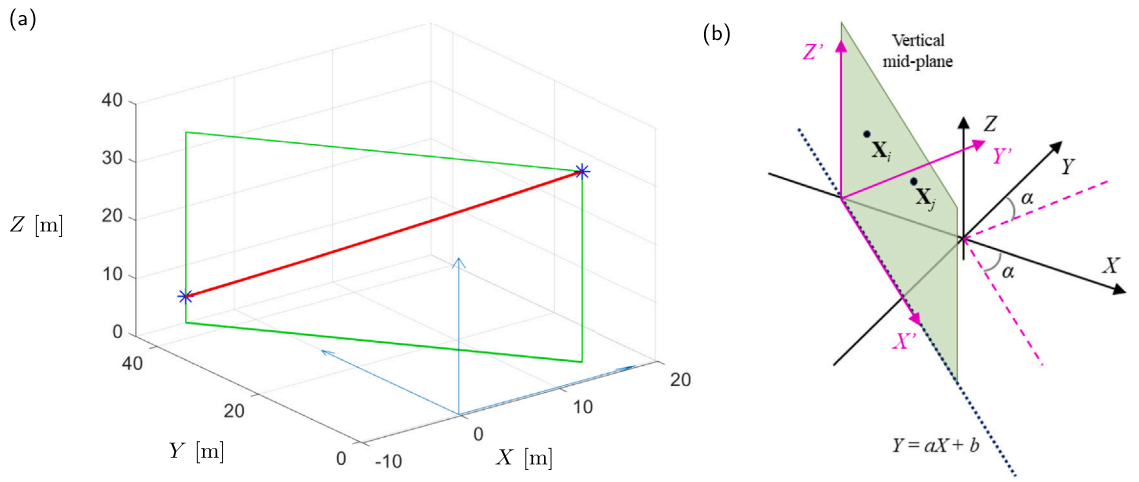

Fig. 4. Identification of the vertical mid-plane of the cable: (a) vertical plane on which the suspended cable hangs; (b) vertical mid-plane orientation and roto-translation of the reference system.

with the Cartesian horizontal plane $\Pi(X,Y)$, described by a straight line equation $Y = aX + b$. On a statistical base, an accurate identification of the coefficients a and b is given by their mean values

$$\hat{a} = \frac{1}{m_R}\sum_{\mathcal{Q}_R} a_{ij}, \qquad \hat{b} = \frac{1}{m_R}\sum_{\mathcal{Q}_R} b_{ij}, \tag{27}$$

where $\mathcal{Q}_R$ is a generic set of m_R pairs (P_i, P_j) of non coincident points $(i \neq j)$, and the coefficients a_{ij} and b_{ij} are identified according to the geometric formulas

$$a_{ij} = \frac{Y_i - Y_j}{X_i - X_j}, \qquad b_{ij} = \frac{X_i Y_j - X_j Y_i}{X_i - X_j} \tag{28}$$

and the set dimension $m_R = n_C(n_C - 1)$ if all the cloud points are employed. Otherwise, $m_R = n_R^2$ if a point cloud model reduction is performed, that is, if a suited subset of $2n_R < n_C$ points is selected to reduce the computational effort. To this end, a proper selection criterion could be to consider n_R points P_i close to the lower cable support $(i = 1, \dots, n_R)$ and n_R points P_j close to the upper support $(j = 1, \dots, n_R)$. Actually, this selection criterion (*Criterion SC1*) tends to maximize the denominators in Eqs. (28) and preserves the identification of coefficients a_{ij} and b_{ij} against the excessive dispersion of results, caused by the high sensitivity to small denominators. As a minor remark, formulas (27) could be further simplified by taking advantage of their natural properties of symmetry ($a_{ij} = a_{ji}$ and $b_{ij} = b_{ji}$).

A suited change of coordinates is required to make the reference system coherent with the assumptions of the direct problem. The ith point $P_i \in \mathcal{P}$ is pointed by the position vector $\mathbf{X}_i' = (X_i', Y_i', Z_i')$ in the new reference system, which is generated by a roto-translational. First, the origin point is translated in the upper support of the cable, whose position is assumed known. Second, a rotation lets the vertical Cartesian plane $\Pi(X', Z')$ of the rotated new reference system coincide with the mid-plane of the point cloud (Fig. 4b). Consequently, the out-of-plane coordinate is considered sufficiently small to be negligible ($Y_i' \simeq 0$) for all the cloud points in the following. Within this geometric framework, the identification of the cubic configuration of the cable from the point cloud is a two-dimensional problem in the plane $\Pi(X', Z')$. The problem can be formulated in nondimensional variables and parameters

$$\xi = \frac{X'}{L}, \qquad \psi = -\frac{Z'}{L}, \qquad \vartheta = \arctan\left(\frac{B}{L}\right), \tag{29}$$

where L and B are here the *measured* horizontal and vertical distances between the cable supports, which can be assumed known, according to the statement of the inverse problem.

With the aim of formally exploiting the analogy with the perturbation-based solution of the direct problem, the cable configuration described by the laser-scanned points can be assumed to be accurately interpolated by the cubic function $\psi(\xi) = \kappa_3 + \kappa_2\xi + \kappa_1\xi^2 + \kappa_0\xi^3$. It may be worth highlighting that (i) in the *direct problem* the cubic nature of the configuration function $y_{[2]}(x)$ is an analytical result, following from the second-order asymptotic approximation of the catenary function, whereas (ii) in the *inverse problem*, the cubic nature of the configuration function $\psi(\xi)$ is a postulate, somehow inspired by the direct problem solution, but essentially based on the fine interpolation accuracy granted by high-order polynomials.

Since two coefficients (κ_3 and κ_2) are determinable by imposing the boundary conditions $\psi(0) = 0$ and $\psi(1) = \tan\vartheta$ (applicable by assuming known the support positions), the cubic function reads

$$\psi(\xi) = \tan\vartheta\,\xi - (\kappa_1 + \kappa_0)\xi + \kappa_1\xi^2 + \kappa_0\xi^3, \tag{30}$$

where the undetermined coefficients κ_0 and κ_1 have to be assessed on the base on experimental measures, since they play the role of known data in the inverse problem of tension identification.

The two coefficients κ_0 and κ_1 can be univocally identified from the knowledge of any pair of two cloud points with nondimensional position vectors $\mathbf{x}_i = (\xi_i, \psi_i)$ and $\mathbf{x}_j = (\xi_j, \psi_j)$, according to the expressions

$$\kappa_{0ij} = \frac{\xi_i\psi_j(1-\xi_i) - \xi_j\psi_i(1-\xi_j) + \Delta(\xi_i,\xi_j)}{\xi_i\,\xi_j(1-\xi_i)(1-\xi_j)(\xi_i-\xi_j)}, \qquad \kappa_{1ij} = \frac{\xi_j\psi_i(1-\xi_j^2) - \xi_i\psi_j(1-\xi_i^2) - \Sigma(\xi_i,\xi_j)}{\xi_i\,\xi_j(1-\xi_i)(1-\xi_j)(\xi_i-\xi_j)}, \tag{31}$$

where the auxiliary quantities

$$\Delta(\xi_i,\xi_j) = \xi_i\,\xi_j(\xi_i-\xi_j)\tan\vartheta, \qquad \Sigma(\xi_i,\xi_j) = \xi_i\,\xi_j(\xi_i+\xi_j)(\xi_i-\xi_j)\tan\vartheta, \tag{32}$$

have been introduced. Therefore, by denoting $\mathcal{Q}_S$ a generic set of m_S pairs (P_i, P_j) of non coincident points ($i \neq j$), a statistically accurate identification of the coefficients κ_0 and κ_1 is given by their mean values

$$\hat{\kappa}_0 = \frac{1}{m_S}\sum_{\mathcal{Q}_S}\kappa_{0ij}, \qquad \hat{\kappa}_1 = \frac{1}{m_S}\sum_{\mathcal{Q}_S}\kappa_{1ij} \tag{33}$$

where the set dimension $m_S = n_C(n_C-1)$, if all the cloud points are employed, or $m_S = n_S^2$ if a suited subset of $2n_S < n_C$ points is selected to reduce the computational effort.

Some mathematical similarities and differences between the identification of the cable mid-plane, based on Eqs. (28), and the identification of the cable configuration, based on Eqs. (31), can be pointed out. Although based on the same logic, the suited selection criteria for the sets $\mathcal{Q}_R$ and $\mathcal{Q}_S$ may differ from each other. Indeed, a proper selection criterion for $\mathcal{Q}_S$ could be to consider two clusters of points. Cluster $\mathcal{P}_1$ includes the n_S points P_i that are closest to the cable abscissa $\xi_1 = (5-\sqrt{5})/10$ (roughly, points ranging between the upper *third* and *fourth* of the cable configuration) Cluster $\mathcal{P}_2$ includes the n_S points P_j that are closest to the cable abscissa $\xi_2 = (5+\sqrt{5})/10$ (roughly, points ranging between the lower *third* and *fourth* of the cable configuration). This selection criterion (*Criterion SC2*) tends to maximize denominators in Eq. (31), with the aim of avoiding excessive dispersion in the statistical identification of coefficients κ_{0ij} and κ_{1ij}. On the other hand, similarly to formula (28) for the identification of the cable mid-plane, formulas in (31) for the identification of the cable configuration could be further simplified by taking advantage of their properties of symmetry ($\kappa_{0ij} = \kappa_{0ji}$ and $\kappa_{1ij} = \kappa_{1ji}$).

Once identified, the coefficients $\hat{\kappa}_0$ and $\hat{\kappa}_1$ suffice to completely assess the configuration of the suspended cable. Finally, the formal analogy between the analytical cubic solution (15) and the geometric cubic interpolation (30) can be invoked to, first, relate the coefficients $\hat{\gamma}_0 = \hat{\kappa}_0$ and $\hat{\gamma}_1 = \hat{\kappa}_1$ and, second, to identify the cable tensions $\hat{H}$ and $\hat{N}(x)$, according to the formulas (19) and (21), respectively. From an application perspective, it may be worth remarking that the quadratic coefficient κ_1 physically describes the larger (constant) contribution to the static curvature of the cable configuration, according to the perturbation scheme. Therefore, an accurate geometric reconstitution of the cable configuration, sufficient to identify even low κ_1-values, is necessary to apply the tension identification procedure to real engineering structures, which are often characterized by highly-tensioned (low sagged) cables. Following the analytical formulation carried out in Section 2.4 for cable-stays, in cable-stayed structures the formal analogy can be established between the experimental cubic function $\psi(\xi)$ and the extended solution $\tilde{y}_{[2]}(\tilde{x})$ defined in (24) to, first, relate the coefficients $\tilde{\beta}_0 = \hat{\kappa}_0$ and $\tilde{\beta}_1 = \hat{\kappa}_1$ and, second, to identify the cable tensions $\hat{H}$ according to the formula (26), where the parameters $\tilde{L}$ and $\tilde{\vartheta}$ indicate the cable span and inclination angle assessed experimentally (that is, including the effects of support displacements).

4. Real-scale application

A pedestrian cable-stayed bridge crossing the Sangone river (namely the Footbridge Albano Zuin in Beinasco, a small city of the Turin province in Italy, see Fig. 5) has been selected as testbed to verify the effectiveness and accuracy of the proposed tension identification approach in real-scale applications. In order to favor reproducibility, this Section illustrates the bridge structure and describes the technical characteristics of the instrumentation for non-contact geometric reconstruction and vibration measurement. Therefore, the identification results are presented and discussed. The result validation is finally provided by comparison with the independent findings of a dynamic (frequency-based) output-only identification method, employing both accelerometer records and image-based vibration signals.

4.1. Bridge description

The cable-stayed footbridge is a steel truss structure, built in 2004. The bridge is characterized by an access ramp and a deck, both supported by steel columns. The ramp and deck are also sustained by a fan system of stay cables anchored at the top of a steel tubular pylon, slightly inclined and 45 m tall, hinged at the base. The steel truss-type beam of the deck is sustained, on the South side, by an access concrete staircase that is located at the center of the access ramp (see Fig. 5a). The deck is 80 m long, 3 m wide and 1.65 m tall, with a 50 m free span featured by slight curvature (in the horizontal plane) and inclination (in the vertical plane). The deck structure is composed of three main tubular members and smaller cross-members. The fan system of pretensioned steel cables is composed by ten spiral strands (with circular 28 mm diameter cross-section) sustaining the access ramp, seven locked coil strands (42 mm diameter) sustaining the deck (see anchorage points of the seven cables supporting the deck in Fig. 5b), and nine locked coil stabilization strands (40 and 42 mm diameters) connecting the pylon to the ground. All the cables are anchored to the ramp and the deck through fork-type lugs with an adjustable threaded rod. In the context of a retrofitting intervention, other data have been made available, including the nominal design values of the cable tensions in the original structural design.

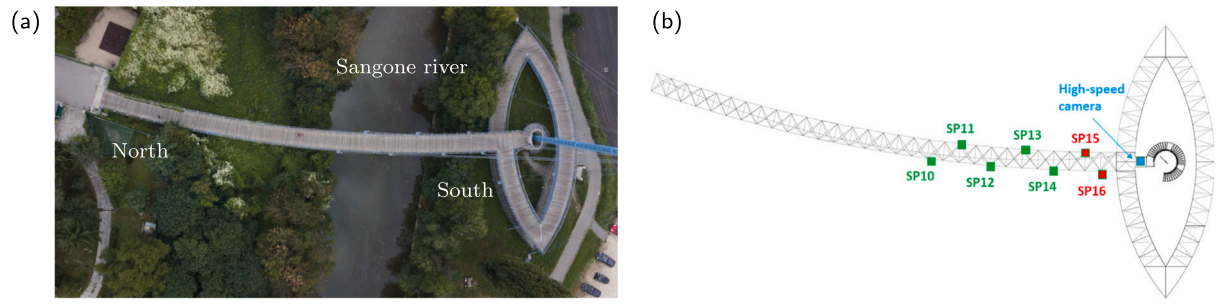

Fig. 5. Footbridge Albano Zuin in Beinasco (Italy): (a) aerial view of the cable-stayed pedestrian bridge, (b) plan view of the bridge, anchorage points of the seven cables supporting the deck and position of the high-speed camera.

Fig. 6. Point cloud model of the Albano Zuin bridge: (a) lateral view of the complete color point cloud model; (b) aerial view of the model region including the seven stay cables supporting the deck.

The three-dimensional geometric configuration of the whole bridge structure has been acquired through the terrestrial laser scanner Cam2 Laser Scanner Focus Faro x 130 (130 m unambiguity interval, 0.6 m–130 m Range Focus3D X 130 HDR, 122000/244000/ 488000/976000 points/s measurement speed, ±2 mm distance error), by carrying out 26 scanning stations for a total of 7 h of acquisition. The merging of the different scans has been performed in the post-processing stage by recognizing homologous points, at least three, based on the recording of GPS positions. The laser scanned data, in combination with the high resolution pictures captured by the integrated camera have allowed to obtain the three-dimensional photorealistic (RGB colored) point cloud model depicted in Fig. 6a. The geometric part of the point cloud model is made up of over 120 million points. The model region including the seven stay cables supporting the deck is illustrated in Fig. 6b.

Dynamic measurements of the stay cables vibrating out-of-plane under impulsive excitation have been acquired by both accelerometers and a high-speed camera. The accelerometer-based instrumentation network included 6 uniaxial piezoelectric wired accelerometers, PCB 393B31 with ICP technology (10.0 V/g sensitivity, 0.5 g peak measurement range, 200 Hz sampling frequency). The camera-based system consisted of the high-speed camera IO Industries Flare 12M125xCL (monochrome, F-mount, 4096 × 3072 resolution, 5.5 × 5.5 μm pixel size, 100–200 fps sampling frequency) and the digital recorder CORE2CLPLUS IO DVR, Core 2, supporting camera link connection up to 4 base inputs and up to 2 full inputs with four 240 GB video storage module (VIDIOMOD240). The camera has been installed on the concrete cantilever of the stairs (in the central area of the ramp) and it has been able to record the out-of-plane vibrations of cables SP15 and SP16 (see Fig. 5b). The dynamic tests have been performed individually for each cable. The displacement time histories have been obtained by using a local approach of the Digital Image Correlation technique (see the Appendix for details).

4.2. Cable tension identification

The tension identification strategy outlined in the previous Sections has been applied to the seven cables supporting the footbridge deck, labeled from SP10 (the longest and least inclined cable) to SP16 (the shortest and most inclined cable) and identified by their anchorage points in Fig. 5b. Other known data (chord length L_c and inclination angle ϑ) of the cables are reported in Table 2. The longest cable SP10 has been selected as case study to discuss some technical issues recurring for all the seven cables.

First, the position data of the point cloud model have been processed to identify the vertical mid-plane of each cable, through the evaluation of the mean coefficients $\hat{a}$ and $\hat{b}$ from Eq. (27). The (a_{ij}, b_{ij})-values have been obtained according to formulas (28) for m_R pairs of points (P_i, P_j) of the subset Q_R (with $m_R = n_R^2$ and $n_R = 100$), defined according to selection criterion *SC1*. Fig. 7a shows all the (a_{ij}, b_{ij})-values obtained for cable SP10. From the qualitative viewpoint, it may be remarkable that all the positions of the (a_{ij}, b_{ij})-values associated to the same point at position $\mathbf{X}_i$ (for $j = 1, \dots, n_R$) are almost perfectly aligned along a certain direction

Table 2
Cable data and results of the static identification strategy from the point cloud model ($n_R = n_S = 100$).

Cable	L_c [m]	ϑ	$\hat{\kappa}_1$	$\hat{\kappa}_0$	$\hat{\delta}$	$\hat{e}$	$\hat{H}$ [kN]	σ^2_H [kN^2]	$\hat{N}$ [kN]	σ^2_N [kN^2]
SP10	52.66	0.5722	−3.30E−02	4.50E−04	8.14E−03	1.18E−04	79.71	3.16E−01	94.82	4.48E−01
SP11	49.56	0.6481	−5.21E−02	8.44E−03	1.27E−02	7.62E−03	46.57	8.05E−02	58.41	1.27E−01
SP12	46.38	0.7309	−1.18E−01	1.51E−04	2.80E−02	−5.05E−03	20.10	2.45E−02	27.00	4.41E−02
SP13	44.45	0.8261	−1.74E−01	2.76E−03	4.03E−02	−5.74E−03	12.53	9.15E−03	18.49	1.99E−02
SP14	42.07	0.9414	−6.28E−02	3.14E−03	1.53E−02	1.89E−03	31.23	1.84E−02	53.05	5.32E−02
SP15	40.93	1.0358	−2.47E−01	1.76E−02	5.62E−02	3.13E−03	8.39	3.18E−03	16.46	1.22E−02
SP16	39.03	1.1118	−1.01E−01	5.78E−04	2.42E−02	−2.20E−03	18.15	5.33E−03	40.96	2.71E−02

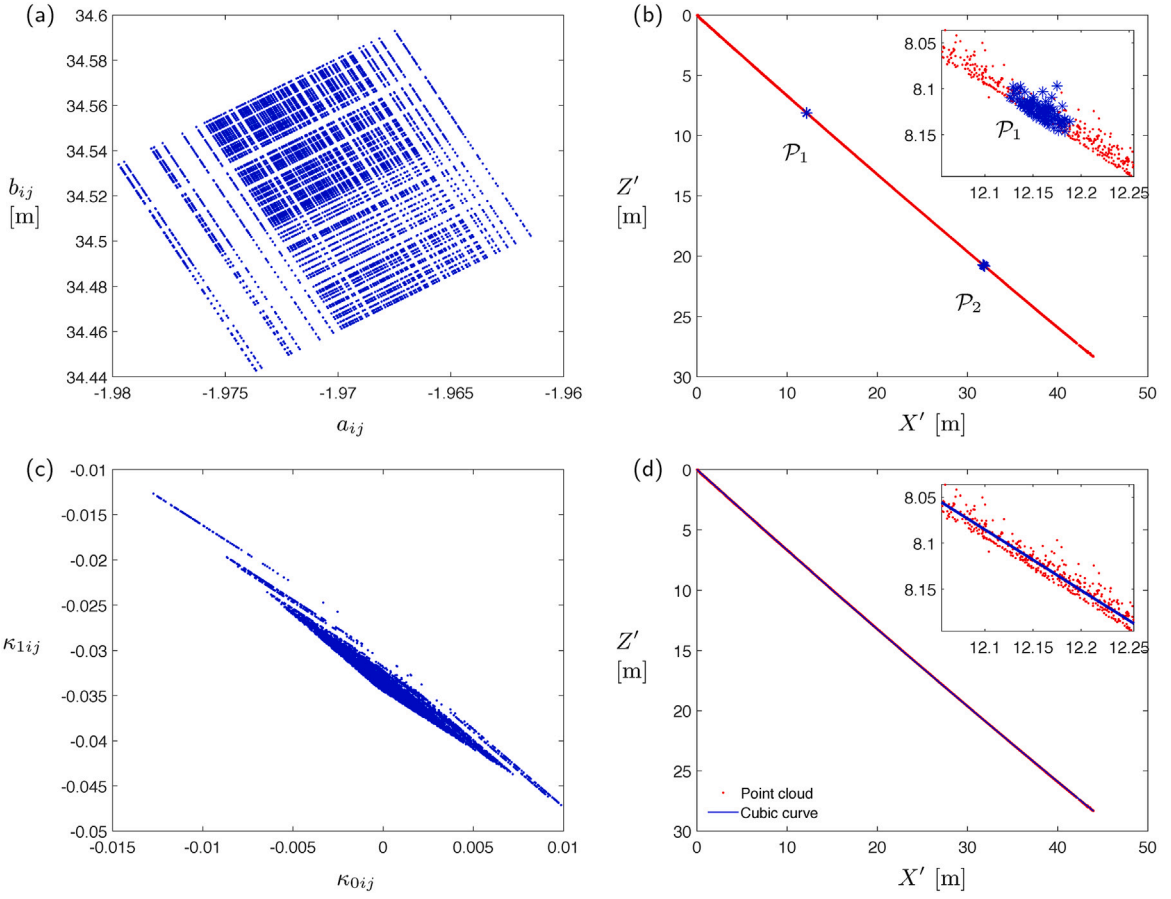

Fig. 7. Configuration of cable SP10 reconstructed from the point cloud model ($n_R = n_S = 100$): (a) coefficients a_{ij}, b_{ij} from the dataset $\mathcal{Q}_R$ of point pairs (P_i, P_j) selected according to the selection criterion *SC1*; (b) point cloud model of cable SP10 (red dots) with point clusters $\mathcal{P}_1$ and $\mathcal{P}_2$ (blue crosses) selected according to the selection criterion *SC2*; (c) coefficients $\kappa_{0ij}, \kappa_{1ij}$ from the dataset $\mathcal{Q}_S$ of point pairs (P_i, P_j) selected according to the selection criterion *SC2*; (d) overlap of the reconstructed cable configuration (blue cubic curve) with the point cloud model (red dots).

of the (a, b)-plane. This behavior can be mathematically justified by the closeness of all the selected points at positions $\mathbf{X}_j$. Indeed, following the selection criterion *SC1*, all the positions $\mathbf{X}_j$ refer to a cluster of close points in the proximity of the upper support. Therefore, the variation of the coefficients $a_{ij}(X_j, Y_j)$ and $b_{ij}(X_j, Y_j)$ associated to the same position $\mathbf{X}_i$ but different positions $\mathbf{X}_j$ can be estimated through the differentials

$$\mathrm{d}a_{ij} = \frac{\partial a_{ij}(X_j, Y_j)}{\partial X_j}\,\mathrm{d}X_j + \frac{\partial a_{ij}(X_j, Y_j)}{\partial Y_j}\,\mathrm{d}Y_j, \qquad \mathrm{d}b_{ij} = \frac{\partial b_{ij}(X_j, Y_j)}{\partial X_j}\,\mathrm{d}X_j + \frac{\partial a_{ij}(X_j, Y_j)}{\partial Y_j}\,\mathrm{d}Y_j, \tag{34}$$

so that, after partial differentiation of the functions defined in Eq. (28), it can be concluded that the ratio $\mathrm{d}b_{ij}/\mathrm{d}a_{ij} = -X_i$ is systematically a constant for each fixed position $\mathbf{X}_i$. This discussion gives qualitative explanation, but also quantitative evaluation (being $\arctan(-X_i)$ the direction angle of the aligned results for the position $\mathbf{X}_i$) for the particular result pattern in the (a, b)-plane.

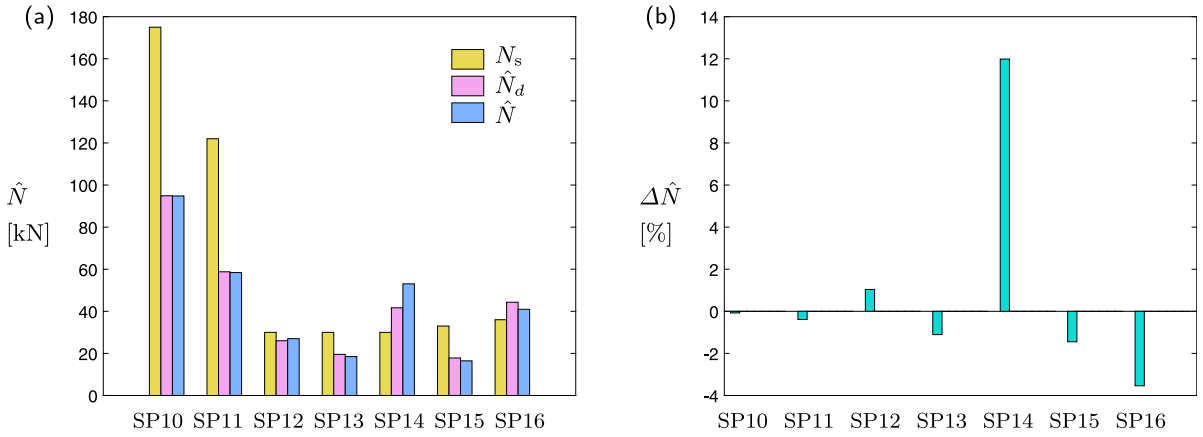

Fig. 8. Cable tension identification of the seven cables supporting the deck from the point cloud model ($n_R = n_S = 100$): (a) comparison of static and dynamic identification results $\hat{N}$ and $\hat{N}_d$ with design values $\hat{N}_s$; (b) difference $\Delta\hat{N}$ between static and dynamic tension identification results.

Subsequently, the position data of the point cloud model in the vertical mid-plane have been further processed to identify the quadratic and cubic coefficients $\hat{\kappa}_0$ and $\hat{\kappa}_1$ defining the cubic configurational function of each cable, according to Eqs. (33). The $(\kappa_{0ij}, \kappa_{1ij})$-values have been obtained according to formulas in (31) for m_S pairs of points (P_i, P_j) of the subset $\mathcal{Q}_S$ (with $m_S = n_S^2$ and $n_S = 100$), defined according to selection criterion *SC2*. To exemplify, the $2n_S$ points belonging to the clusters $\mathcal{P}_1$ and $\mathcal{P}_2$ selected for cable SP10 are marked by blue crosses in Fig. 7b. The corresponding $(\kappa_{0ij}, \kappa_{1ij})$-values in the (κ_0, κ_1)-plane are illustrated in Fig. 7c. Similarly to the (a_{ij}, b_{ij})-identification, all the positions of the $(\kappa_{0ij}, \kappa_{1ij})$-values associated to the same point at position $\mathbf{X}_i$ (for $j = 1, \dots, n_R$) are almost perfectly aligned along a certain direction of the (κ_0, κ_1)-plane. Again, a qualitative physical explanation is related to the closeness of all the positions $\mathbf{X}_j$. The explanation can be supported by a quantitative mathematical argument based on evaluating the differentials $\mathrm{d}\kappa_{0ij}(X_j, Y_j)$ and $\mathrm{d}\kappa_{1ij}(X_j, Y_j)$. Specifically, it can be proved that the ratio $\mathrm{d}\kappa_{1ij}/\mathrm{d}\kappa_{0ij}$ is systematically equal to the constant $-(\xi_i + 1)$ for each fixed position $\mathbf{X}_i$. Fig. 7d illustrates the cubic curve (blue line) univocally defined by the identified coefficients κ_0 and κ_1. The high fitting accuracy can be appreciated from the comparison with the point cloud model (red dots).

Finally, the horizontal reaction $\hat{H}$ and the axial tension $\hat{N}$ are respectively identified by using Eqs. (19) and (21), where only the lowest order term has been considered. The complete outputs of the identification procedure for all the seven stays, including both intermediate results (configurational coefficients $\hat{\kappa}_0$ and $\hat{\kappa}_1$) and final results (sag-to-span ratio $\hat{\delta}$, horizontal reaction $\hat{H}$ and axial tension $\hat{N}$) are summarized in Table 2. Considering than the identified quantities $\hat{\delta}$, $\hat{H}$, $\hat{N}$ can be regarded as mean values over the criterion-dependent subset $\mathcal{Q}_S$ of m_S point pairs in the cloud model, the corresponding variances σ_H^2 and σ_N^2 have been determined to give an account of the result dispersion. Furthermore, the effects of different reductions of the point cloud model (different m_S-values) are discussed in one of the next subsections.

Focusing first on the quadratic configurational coefficient $\hat{\kappa}_1$, very low-amplitude mean values ranging from $\hat{\kappa}_1 = -0.0330$ (longest cable SP10) to $\hat{\kappa}_1 = -0.247$ (short cable SP15) have been identified, with minimal dispersion of the identification results (considering that the corresponding variances, here not reported for the sake of synthesis, are two or three orders of magnitude lower than the mean). This finding confirms that the geometric precision and resolution of the point cloud model are sufficient for the tension identification in all the low-sagged cables of the footbridge. As regards cubic coefficient κ_0, ranging between 0.0002 (long cable SP12) and 0.0176 (short cable SP15), the identified values are at least one or two orders of magnitude lower than those of coefficient κ_1. This experimental evidence supports a posteriori the ordering of the parameters postulated a priori to develop the perturbation-based solution of the direct problem.

Focusing on the horizontal reaction $\hat{H}$ and axial tension $\hat{N}$, a high variability of mean values, ranging from $\hat{N} = 94.82$ kN (longest cable SP10) to $\hat{N} = 16.46$ kN (short cable SP15), has been found. The general quality of the tension identification is evidenced by the minimal dispersion of the results, described by variances ranging from $\sigma_N^2 = 0.448$ kN^2 (longest cable SP10) to $\sigma_N^2 = 0.0122$ kN^2 (short cable SP15), and is also confirmed by the very low values attained by the independent quantity $\hat{e}$ (maximum absolute value $|\hat{e}| = 0.008$), expressing the relative difference between the $\hat{H}$-identifications based on the cubic and quadratic configuration coefficients. From the physical viewpoint, the identified scenario clearly shows that the two longest cables are characterized by the highest axial tensions, also corresponding to the largest static curvatures and midspan sags. Fig. 8 shows the statically identified tensions $\hat{N}$ (blue bars) compared with the nominal design values $\hat{N}_s$ (yellow bars) for all the cables. The comparison highlights a certain tension loss in the majority of the cables (Fig. 8a). The largest losses, probably attributable to long-term phenomena of stress relaxation, can be recognized in the two longest, highly tensioned cables. Shorter cables exhibit lower tension losses, or even moderate tension increments, probably caused by time-dependent redistributions of internal forces in the highly hyperstatic structural system.

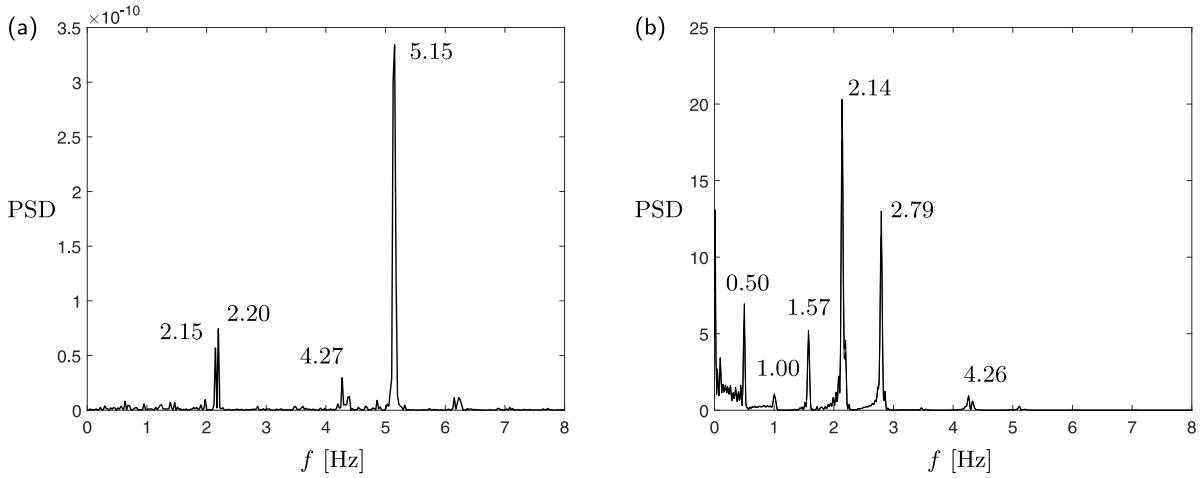

Fig. 9. Identification of out-of-plane frequencies based on peak-picking method for cable SP15: (a) PSD of accelerometer signal (acceleration); (b) PSD of camera signal (displacement).

Table 3
Frequency-based cable tension identification.

Cable	f_1 [Hz]	f_2 [Hz]	f_3 [Hz]	f_4 [Hz]	f_5 [Hz]	$\hat{N}_d$ [kN]	$\Delta\hat{N}$ [%]
SP10	–	–	2.76	3.69	–	94.89	−0.08
SP11	–	–	–	3.08	3.83	58.78	−0.39
SP12	–	–	–	–	2.73	26.02	1.04
SP13	–	–	–	1.98	–	19.54	−1.11
SP14	–	–	–	3.05	–	41.68	11.99
SP15	0.50	1.00	1.57	2.14	2.79	17.83	−1.45
SP16	0.84	1.69	2.58	3.44	–	44.31	−3.54

4.3. Validation of results

An independent identification of cable tension has been performed by using a reliable dynamic method based on the analytical inversion of the frequency-to-tension relationship. According to the classic cable model [1], which assumes parabolic static profile, linear elastic behavior and negligible longitudinal inertia, the linear frequencies and modes characterizing the undamped out-of-plane motion in the small amplitude oscillation range are sag-independent. Moreover, the circular (square) frequency ω_k^2 depend on the constant axial tension N and the uniformly distributed mass density m according to the (string-like) relation

$$\omega_k^2 = 4\pi^2 f_k^2 = \frac{k^2\pi^2}{L_c^2}\frac{N}{m} \tag{35}$$

where $k \in \mathbb{N}$ is the mode number. The relation can be easily inverted to assess the cable tension N if a frequency f_k is experimentally identified and the other quantities are known.

The dynamic identification of the lowest cable frequencies has been based on the so-called *peak-picking* method, which consists in selecting the frequency f_k corresponding to the kth peak in the Power Spectral Density (PSD) function associated to displacement or acceleration time histories. In the absence of sufficient ambient excitation, the free out-of-plane motion of the cables has been activated by hammer impacts, and subsequently recorded by the high-speed camera (displacements) and the accelerometers (accelerations). Particular care has been taken to discard time windows of high amplitude oscillations, in order to avoid possible frequency variations due to nonlinearities. The modal damping values, estimated by the method of logarithmic decrement, have turned out to be sufficiently small to permit long acquisition records and not to alter the free oscillation frequencies. As expected, the displacement signals captured by the high-speed camera have provided higher and easier distinguishable peaks in the Power Spectral Density functions, especially in the low-frequency range. To exemplify, the PSD functions of selected acceleration and displacement time histories of the cable SP15 are illustrated in Fig. 9. Compared with the acceleration PSD function, the displacement PSD function allows to easily recognize the equispaced distribution of high frequency peaks typical of the linear (f_k, k)-relations.

The frequencies identified for all the cables are listed in Table 3, together with the axial tensions $\hat{N}_d$ identified according to the dynamic method by using the lowest mode. The dynamically identified tensions $\hat{N}_d$ (red bars) are also compared with the statically identified tensions $\hat{N}$ (blue bars) in Fig. 8a. The comparison highlights an excellent agreement between the results, which can be quantitatively evaluated by the nondimensional quantity

$$\Delta\hat{N} = \frac{\hat{N} - \hat{N}_d}{\hat{N}_d} \tag{36}$$

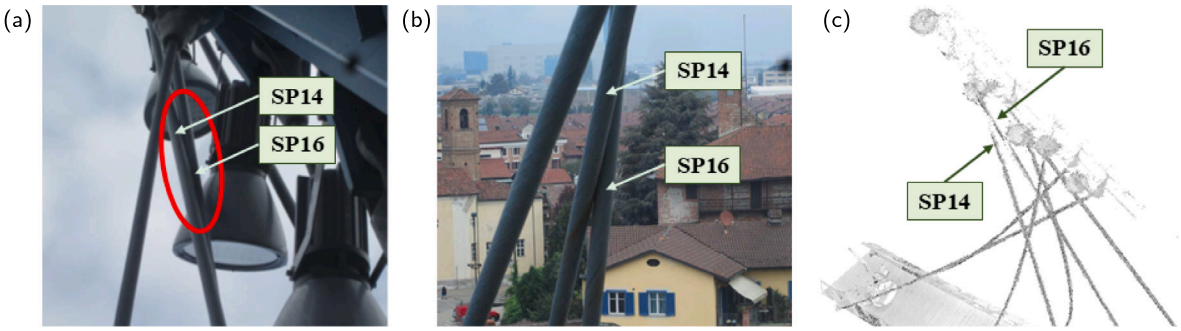

Fig. 10. Contact point between cables SP14 and SP16: (a,b) detail pictures; (c) point cloud region.

which turns out to be less than 0.5% for the longest cables (SP10, SP11), and less than 1.5% for other shorter cables (SP12, SP13, SP15). The $\Delta\hat{N}$-values determined for each cable are reported in Table 3 and also plotted in Fig. 8b. From the mathematical viewpoint, it is worth remarking that the static results do not show any marked tendency of underestimation or overestimation compared to the dynamic results. This evidence indicates that the static procedure is not affected by undesired systematic bias. Lower agreement is found for cable SP16 ($\Delta\hat{N} \simeq -3.5\%$) and – especially – cable SP14 ($\Delta\hat{N} \simeq 12\%$). A tentative explanation for this disagreement can be traced to constructional issues, since the upper ends of cable SP14 and SP16 are so close enough to touch each other during small-amplitude motions (as illustrated by pictures and point cloud data in Fig. 10). On the one hand, the contact is suspected of creating a non quantifiable dynamic interaction between the two cables (due to the presence of a non-smooth unilateral inter-cable constraint) and, consequently, disturbing the dynamic tension identification, based on the hypothesis of free undamped oscillations. On the other hand, the contact point may have determined local losses of geometric accuracy in the point cloud description of the two cables. Since the employment of the selection criteria *SC1* and *SC2* has allowed to exclude the inter-cable contact region from the data, the tension values resulting from the static identification procedure are expected to be more reliable.

4.4. Effects of point cloud model reduction

The proposed strategy for tension identification basically relies on the statistical treatment of the point dataset $\mathcal{P}$ realizing the cloud model. Naturally, high-dimensional models – like those acquired by modern high-resolution laser scanners – may slow down the numerical procedures of data processing or still require considerable computational resources. Therefore, model reductions targeted at selecting particular data subsets according to proper selection criteria (*SC1* and *SC2*) can be conveniently adopted to reduce the computational burden without compromising the result accuracy. According to these considerations, some parametric analyses have been carried to assess how the model dimension influences the tension identification. The number $n_R = n_S = n$ has been considered as synthetic parameter describing the point cloud dimension. Indeed, larger n-value (up to $n_{\max} = 3200$) allows to increase the dimension of the sets $\mathcal{Q}_R$ and $\mathcal{Q}_S$ used to identify the mid-plane and the configurational coefficients of the cable.

The first point of interest concerns the effect of different point cloud reductions on the n-dependent geometric size of the clusters $\mathcal{P}_1$ and $\mathcal{P}_2$ used to identify the configurational coefficients according to the selection criterion *SC2*. This sizes can be estimated by defining the quantities

$$\hat{\xi}_1 = \frac{1}{n}\sum_{i=1}^{n}(\xi_i - \xi_1), \qquad \hat{\xi}_2 = \frac{1}{n}\sum_{j=1}^{n}(\xi_j - \xi_2), \tag{37}$$

expressing the mean horizontal distance $\hat{\xi}_1$ of the n points $P_i \in \mathcal{P}_1$ from the abscissa ξ_1 and the mean horizontal distance $\hat{\xi}_2$ of the n points $P_j \in \mathcal{P}_2$ from the abscissa ξ_2. The results are reported in Fig. 11a,b for the investigation range $50 \le n \le n_{\max}$. The major remark is that the mean distances $\hat{\xi}_1$ and $\hat{\xi}_2$ remain systematically low (specifically $\hat{\xi}_1 < 0.002$ and $\hat{\xi}_2 < 0.001$ for the worst case related to cable SP12) up to large n-values (namely up to $n \simeq 1600$). A rapid increment of the mean distances occurs only for larger n-values (e.g. $n_{\max} = 3200$). This finding confirms that the selection criterion *SC2* can be applied with mathematical consistency (closeness of the clusters $\mathcal{P}_1$ and $\mathcal{P}_2$ to the points ξ_1 and ξ_2) without loss of statistical accuracy in the identification (poor dataset due to excessive model reduction). Furthermore, the evaluation of the mean horizontal distances shows that the density of the point cloud is lower for cable SP12 (the size of the clusters $\mathcal{P}_1$ and $\mathcal{P}_2$ is higher compared to other cables). Consequently, the quality of point cloud data may not be the same for all cables because it depends on the position of the scanned elements with respect to the laser scanner.

The second point of interest relates to the effect of different point cloud reductions on the static identification of axial tensions. To this aim, the identified axial tension can be considered as n-dependent variable $\hat{N}(n)$ and the nondimensional *identification difference*

$$\Delta\hat{N}_n = \frac{\hat{N}(n) - \hat{N}(n_{\max})}{\hat{N}(n_{\max})}. \tag{38}$$

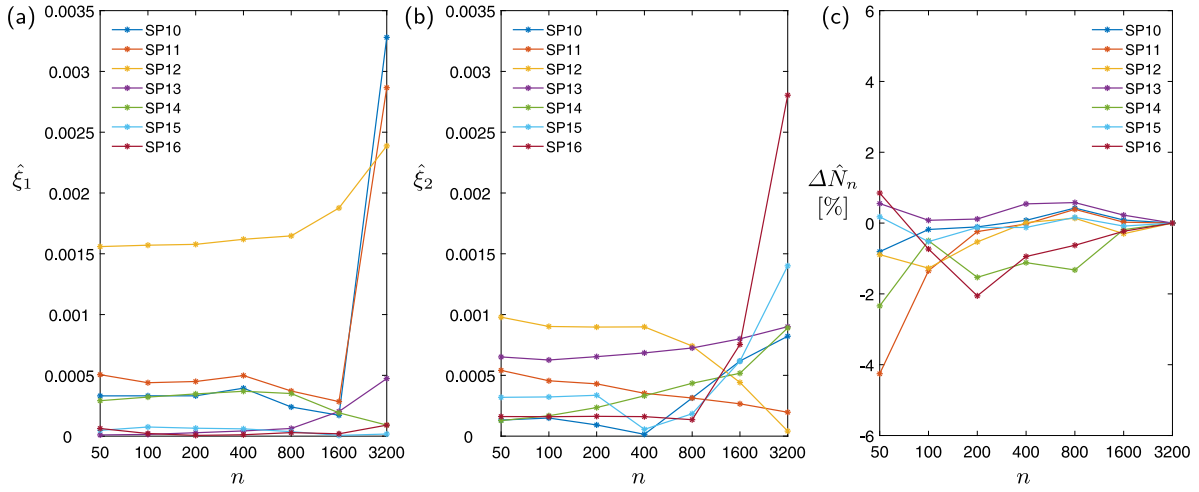

Fig. 11. Effects of the point cloud model reduction on the static identification results: (a) size $\hat{\xi}_1$ versus dimension n of the point cluster $\mathcal{P}_1$; (a) size $\hat{\xi}_2$ versus dimension n of the point cluster $\mathcal{P}_2$; (c) tension identification difference $\Delta\hat{N}_n$ versus the n-dependent point cloud reduction.

can be introduced to evaluate how more or less reduced point cloud model influences the identification. The results are reported in Fig. 11c for the investigation range $50 \leq n \leq n_{\max}$. The major remark is that the identification difference shows small variations (specifically $|\Delta\hat{N}_n| < 2\%$) for all the cables and over almost the entire investigation range (namely for $n > 50$). This finding confirms that the selection criterion *SC2* applied with $n = 100$ in the previous sections would be minimally affected by considering larger datasets given by less reduced point cloud models.

5. Conclusions

A novel strategy for identifying the axial tension in inclined, sagged and perfectly flexible cables has been proposed, which virtuously combines physical–mathematical models with contactless digital technologies. The primary idea, conceived within the framework of theoretical structural mechanics, is that analytical – although asymptotically approximate – solutions of the differential problem governing the static cable equilibrium can contribute decisively to the recognition of highly sensitive tension-dependent configurational quantities. The complementary idea, developed in the rapidly-evolving field of new digital technologies, is that modern techniques of laser scanning can provide three-dimensional descriptions of the cable configuration with unprecedented levels of geometric accuracy and resolution.

First, a mono-parametric perturbation method has been formulated to achieve a suitable analytical (polynomial) solution that parametrically approximates the static equilibrium configuration assumed by a suspended perfectly flexible cable under self-weight (*direct problem*). From a methodological viewpoint, the peculiarity of the perturbation method is that only unknown quantities require to be ordered in power series of a small bookkeeping parameter. As a major finding, the polynomial coefficients of the configurational function have been analytically related to cable tension. The inversion of the coefficient-to-tension relations provides parametric formulas for tension identification (*inverse problem*). Although the development of the perturbation scheme has been limited to lower orders, its extension to higher orders is expected to improve the analytical approximation to the desired accuracy. The identification strategy has also been demonstrated to be directly applicable to cable stays used as stiffening or supporting members in cable-stayed structures, by virtue of minor reparameterizations of the inverse problem data.

Second, a numerical algorithm has been outlined for the statistical reconstruction of the configurational coefficients from the experimental point cloud model acquired by a laser scanner (*configuration reconstruction*). The algorithm differs slightly from standard interpolation schemes because of the physically-informed constraints, which affect the boundary conditions and selection criteria for reduced datasets.

Finally, the identification strategy has been applied on a real-scale structure of engineering interest. Specifically, the axial tensions in the stays of a cable-stayed footbridge have been identified. Qualitative and quantitative issues have been discussed to physically justify and mathematically interpret the systematic patterns characterizing the intermediate and final results in the identified parameter space. The mean identification outputs have been found to be associated with low dispersion throughout the algorithmic procedure, whereas the final results have been verified to be minimally affected by dimensional reductions in the input dataset based on mathematical criteria. Therefore, the strategy has been successfully validated by the excellent agreement of the results with an independent output-only dynamic approach, implementing a frequency-based tension identification.

Considering the advantages and disadvantages, the proposed static strategy of tension identification is limited by the impossibility of monitoring time-varying cable forces owing to dynamic phenomena. Nonetheless, in addition to being theoretically consistent and technologically feasible, the static strategy has the competitive advantage of not requiring any artificial or environmental source of excitation. Thus, it is not subject to the limitations imposed by dynamic identification methods, such as knowledge of excitation (input–output methods) or assumptions about its statistical properties (output-only methods).

Declaration of competing interest

The authors declare the following financial interests/personal relationships which may be considered as potential competing interests: Vincenzo Gattulli reports financial support was provided by Government of Italy Ministry of Education University and Research.

Data availability

Data will be made available on request.

Acknowledgments

This research was supported by co-funding of the European Union - The National Recovery and Resilience Plan (NRRP) – Mission 4 Component 2 Investment 1.4 - NextGeneration EU Project - Project "MOST-Sustainable Mobility Center" - CUP B83C22002900007 - Spoke 7. This research was in part sponsored by the NATO Science for Peace and Security Programme under grant id. G5924.

Appendix

A.1. Image-based vibration measurements

Dynamic image analysis is a non-contact digital measurement technique, which has been proved to be convenient and efficient for vibration recording and structural identification. The technical convenience and efficiency can be attributed to the current availability of high resolution and high-speed cameras and the development of increasingly performing visual tracking algorithms [69,70]. Different visual tracking techniques can be applied to extract displacements from the matching of different image objects [71]. *Template matching* techniques perform the sliding of a selected Region of Interest (ROI) across series of images; to find the best matching, their similarity is evaluated through the minimization of the sum of squared differences or the maximization of the cross-correlation. *Feature tracking* algorithms find the similarity of small region of the image characterized by distinct features (intensities, gradients, textures) which remain unchanged during the registration by evaluating Euclidean or Hamming distances. With *geometry matching* methods, the tracking is performed on geometry objects, such as edge, square, circle.

One of the most used techniques in the field of structural dynamics, and referred to in this work, is the Digital Image Correlation (DIC), which is based on a template matching approach. According to this technique, the motion is determined by considering two image frames with gray scale intensity $I(\mathbf{x},t)$ and $I(\mathbf{x},t+\Delta t)$ of each pixel $\mathbf{x}$ shot at times t and $t+\Delta t$. Let $\mathbf{u}(\mathbf{x})$ be the displacement, between the two image frames, of a pixel at location $\mathbf{x}$ with intensity $I(\mathbf{x},t)$, the equation

$$I(\mathbf{x},t) = I(\mathbf{x}+\mathbf{u}(\mathbf{x}),t+\Delta t) \tag{A.1}$$

corresponds to the local gray level conservation. This is a scalar equation with n unknowns ($n = 2$ in 2D case, $n = 3$ in 3D case) which cannot be solved at pixel level. Therefore, the registration is performed on a set of pixels referred to as Zone Of Interest (ZOI), or on the Region Of Interest (ROI) itself [72]. A norm between the signal difference is chosen

$$\eta_c^2(\mathbf{u}) = \sum_{\Omega} \left[I(\mathbf{x},t) - I(\mathbf{x}+\mathbf{u}(\mathbf{x}),t+\Delta t) \right]^2 \tag{A.2}$$

where Ω is the considered domain (ZOI or ROI) where the registration is performed. The displacements are obtained through the minimization of η_c^2 with respect to $\mathbf{u}$. If Eq. (A.2) is written on ZOI, by assuming that $\mathbf{u}$ is a rigid body translation, the minimization of such norm corresponds to maximize the correlation between the two image frames.

References

[1] H.M. Irvine, Cable Structures, The MIT Press, 1981.
[2] G. Rega, Nonlinear vibrations of suspended cables – Part I: Modeling and analysis, Appl. Mech. Rev. 57 (6) (2004) 443–478.
[3] G. Rega, Nonlinear vibrations of suspended cables – Part II: Deterministic phenomena, Appl. Mech. Rev. 57 (6) (2004) 479–514.
[4] R.A. Ibrahim, Nonlinear vibrations of suspended cables – Part III: Random excitation and interaction with fluid flow, Appl. Mech. Rev. 57 (6) (2004) 515–549.
[5] A. Luongo, D. Zulli, Mathematical Models of Beams and Cables, John Wiley & Sons, 2013.
[6] A.B. Mehrabi, In-service evaluation of cable-stayed bridges, overview of available methods and findings, J. Bridge Eng. 11 (6) (2006) 716–724.
[7] N.C. Perkins, Modal interactions in the non-linear response of elastic cables under parametric/external excitation, Int. J. Non-Linear Mech. 27 (2) (1992) 233–250.
[8] V. Gattulli, M. Lepidi, F. Potenza, U. Di Sabatino, Modal interactions in the nonlinear dynamics of a beam–cable–beam, Nonlinear Dynam. 96 (4) (2019) 2547–2566.
[9] P. Zhou, G. Zhou, Z. Zhu, Z. He, X. Ding, C. Tang, A review of non-destructive damage detection methods for steel wire ropes, Appl. Sci. 9 (13) (2019) 2771.

[10] E. Caetano, Characterisation and assessment of damage in cable structures, J. Civ. Struct. Health Monit. 12 (6) (2022) 1267–1283.
[11] J. Lardies, T. Minh-Ngi, Modal parameter identification of stay cables from output-only measurements, Mech. Syst. Signal Process. 25 (1) (2011) 133–150.
[12] M. Lepidi, V. Gattulli, F. Vestroni, Static and dynamic response of elastic suspended cables with damage, Int. J. Solids Struct. 44 (25–26) (2007) 8194–8212.
[13] M. Lepidi, V. Gattulli, F. Vestroni, Damage identification in elastic suspended cables through frequency measurement, J. Vib. Control 15 (6) (2009) 867–896.
[14] S. Cho, J. Yim, S.W. Shin, H.-J. Jung, C.-B. Yun, M.L. Wang, Comparative field study of cable tension measurement for a cable-stayed bridge, J. Bridge Eng. 18 (8) (2013) 748–757.
[15] A. Pacitti, M. Peigney, F. Bourquin, W. Lacarbonara, Cable tension identification via nonlinear static inverse problem, Struct. Health Monit. 20 (2) (2021) 546–566.
[16] J.C. Russell, T. Lardner, Experimental determination of frequencies and tension for elastic cables, J. Eng. Mech. 124 (10) (1998) 1067–1072.
[17] B.H. Kim, T. Park, H. Shin, T.-Y. Yoon, A comparative study of the tension estimation methods for cable supported bridges, Int. J. Steel Struct. 7 (1) (2007) 77–84.
[18] J.R. Casas, A combined method for measuring cable forces: the cable-stayed alamillo bridge spain, Struct. Eng. Int. 4 (4) (1994) 235–240.
[19] R. Geier, G. De Roeck, R. Flesch, Accurate cable force determination using ambient vibration measurements, Struct. Infrastruct. Eng. 2 (1) (2006) 43–52.
[20] H. Zui, T. Shinke, Y. Namita, Practical formulas for estimation of cable tension by vibration method, J. Struct. Eng. 122 (6) (1996) 651–656.
[21] Z. Fang, J.-q. Wang, Practical formula for cable tension estimation by vibration method, J. Bridge Eng. 17 (1) (2012) 161–164.
[22] W.-X. Ren, G. Chen, W.-H. Hu, et al., Empirical formulas to estimate cable tension by cable fundamental frequency, Struct. Eng. Mech. 20 (3) (2005) 363–380.
[23] X. Zhang, H. Xu, M. Cao, D. Sumarac, Y. Lu, J. Peng, In-plane free vibrations of small-sag inclined cables considering bending stiffness with applications to cable tension identification, J. Sound Vib. 544 (2023) 117394.
[24] G. Ricciardi, F. Saitta, A continuous vibration analysis model for cables with sag and bending stiffness, Eng. Struct. 30 (5) (2008) 1459–1472.
[25] M. Javanbakht, S. Cheng, F. Ghrib, Impact of support stiffness on the performance of negative stiffness dampers for vibration control of stay cables, Struct. Control Health Monit. 27 (10) (2020) e2610.
[26] F. Foti, M. Geuzaine, V. Denoël, On the identification of the axial force and bending stiffness of stay cables anchored to flexible supports, Appl. Math. Model. 92 (2021) 798–828.
[27] B.H. Kim, T. Park, Estimation of cable tension force using the frequency-based system identification method, J. Sound Vib. 304 (3–5) (2007) 660–676.
[28] W. Liao, Y. Ni, G. Zheng, Tension force and structural parameter identification of bridge cables, Adv. Struct. Eng. 15 (6) (2012) 983–995.
[29] L. Ma, A highly precise frequency-based method for estimating the tension of an inclined cable with unknown boundary conditions, J. Sound Vib. 409 (2017) 65–80.
[30] S. Cho, J.P. Lynch, J.-J. Lee, C.-B. Yun, Development of an automated wireless tension force estimation system for cable-stayed bridges, J. Intell. Mater. Syst. Struct. 21 (3) (2010) 361–376.
[31] X. Zhang, J. Peng, M. Cao, D. Damjanović, W. Ostachowicz, Identification of instantaneous tension of bridge cables from dynamic responses: STRICT algorithm and applications, Mech. Syst. Signal Process. 142 (2020) 106729.
[32] H. Li, F. Zhang, Y. Jin, Real-time identification of time-varying tension in stay cables by monitoring cable transversal acceleration, Struct. Control Health Monit. 21 (7) (2014) 1100–1117.
[33] Y. Yang, S. Li, S. Nagarajaiah, H. Li, P. Zhou, Real-time output-only identification of time-varying cable tension from accelerations via complexity pursuit, J. Struct. Eng. 142 (1) (2016) 04015083.
[34] Y. Bao, Z. Shi, J.L. Beck, H. Li, T.Y. Hou, Identification of time-varying cable tension forces based on adaptive sparse time-frequency analysis of cable vibrations, Struct. Control Health Monit. 24 (3) (2017) e1889.
[35] A. Cunha, E. Caetano, Dynamic measurements on stay cables of cable-stayed bridges using an interferometry laser system, Exp. Tech. 23 (1999) 38–43.
[36] A.B. Mehrabi, S. Farhangdoust, A laser-based noncontact vibration technique for health monitoring of structural cables: background, success, and new developments, Adv. Acoust. Vib. 2018 (2018) 8640674.
[37] C. Gentile, A. Cabboi, Vibration-based structural health monitoring of stay cables by microwave remote sensing, Smart Struct. Syst. 16 (2) (2015) 263–280.
[38] Z. Yu, S. Shao, N. Liu, Z. Zhou, L. Feng, P. Du, J. Tang, Cable tension identification based on near field radiated acoustic pressure signal, Measurement 178 (2021) 109354.
[39] D. Jana, S. Nagarajaiah, Y. Yang, Computer vision-based real-time cable tension estimation algorithm using complexity pursuit from video and its application in fred-hartman cable-stayed bridge, Struct. Control Health Monit. 29 (9) (2022) e2985.
[40] S. Wangchuk, D.M. Siringoringo, Y. Fujino, Modal analysis and tension estimation of stay cables using noncontact vision-based motion magnification method, Struct. Control Health Monit. 29 (7) (2022) e2957.
[41] Y. Zhou, Z. Xiang, X. Zhang, Y. Wang, D. Han, C. Ying, Mechanical state inversion method for structural performance evaluation of existing suspension bridges using 3d laser scanning, Comput.-Aided Civ. Infrastruct. Eng. 37 (5) (2022) 650–665.
[42] A.H. Nayfeh, Introduction to Perturbation Techniques, John Wiley & Sons, 1981.
[43] A.P. Seyranian, A.A. Mailybaev, Multiparameter Stability Theory with Mechanical Applications, Volume 13, World Scientific, 2003.
[44] R.H. Rand, D. Armbruster, Perturbation Methods, Bifurcation Theory and Computer Algebra, Volume 65, Springer Science & Business Media, 2012.
[45] A. Luongo, On the use of the multiple scale method in solving 'difficult'bifurcation problems, Math. Mech. Solids 22 (5) (2017) 988–1004.
[46] M. Hajj, J. Fung, A. Nayfeh, S. Fahey, Damping identification using perturbation techniques and higher-order spectra, Nonlinear Dynam. 23 (2) (2000) 189–203.
[47] G. Kerschen, K. Worden, A.F. Vakakis, J.-C. Golinval, Past, present and future of nonlinear system identification in structural dynamics, Mech. Syst. Signal Process. 20 (3) (2006) 505–592.
[48] Lepidi M., Multi-parameter perturbation methods for the eigensolution sensitivity analysis of nearly-resonant non-defective multi-degree-of-freedom systems, J. Sound Vib. 332 (4) (2013) 1011–1032.
[49] W. Lacarbonara, B. Carboni, G. Quaranta, Nonlinear normal modes for damage detection, Meccanica 51 (11) (2016) 2629–2645.
[50] E. Lofrano, A. Paolone, M. Vasta, A perturbation approach for the identification of uncertain structures, Int. J. Dyn. Control 4 (2) (2016) 204–212.
[51] M. Lepidi, A. Bacigalupo, Parametric design of the band structure for lattice materials, Meccanica 53 (3) (2018) 613–628.
[52] V. Denoël, E. Detournay, Multiple scales solution for a beam with a small bending stiffness, J. Eng. Mech. 136 (1) (2010) 69–77.
[53] A. Luongo, D. Zulli, Statics of shallow inclined elastic cables under general vertical loads: A perturbation approach, Mathematics 6 (2) (2018) 24.
[54] M. Triantafyllou, The dynamics of taut inclined cables, Quart. J. Mech. Appl. Math. 37 (3) (1984) 421–440.
[55] C. Lee, N.C. Perkins, Three-dimensional oscillations of suspended cables involving simultaneous internal resonances, Nonlinear Dynam. 8 (1) (1995) 45–63.
[56] A.H. Nayfeh, H.N. Arafat, C.-M. Chin, W. Lacarbonara, Multimode interactions in suspended cables, J. Vib. Control 8 (3) (2002) 337–387.
[57] A. Berlioz, C.-H. Lamarque, Nonlinear vibrations of an inclined cable, J. Vib. Acoust. 127 (4) (2004) 315–323.
[58] P. Yu, Y. Desai, A. Shah, N. Popplewell, Three-degree-of-freedom model for galloping, part i: Formulation, J. Eng. Mech. 119 (12) (1993) 2404–2425.
[59] P. Yu, Y. Desai, N. Popplewell, A. Shah, Three-degree-of-freedom model for galloping, part ii: Solutions, J. Eng. Mech. 119 (12) (1993) 2426–2448.
[60] A. Luongo, G. Piccardo, Non-linear galloping of sagged cables in 1: 2 internal resonance, J. Sound Vib. 214 (5) (1998) 915–940.
[61] P. Warnitchai, Y. Fujino, B.M. Pacheco, R. Agret, An experimental study on active tendon control of cable-stayed bridges, Earthq. Eng. Struct. Dyn. 22 (2) (1993) 93–111.

[62] V. Gattulli, M. Pasca, F. Vestroni, Nonlinear oscillations of a nonresonant cable under in-plane excitation with a longitudinal control, Nonlinear Dynam. 14 (2) (1997) 139–156.
[63] M. Lepidi, Catenary solutions for inextensible cables: a perturbation-based high-order approximation, in: Dynamics and Aerodynamics of Cables, ISDAC 2023, in: Lecture Notes in Civil Engineering, vol. 399, Springer, 2023.
[64] Y. Fujino, P. Warnitchai, B. Pacheco, An experimental and analytical study of autoparametric resonance in a 3dof model of cable-stayed-beam, Nonlinear Dynam. 4 (2) (1993) 111–138.
[65] V. Gattulli, M. Lepidi, Nonlinear interactions in the planar dynamics of cable-stayed beam, Int. J. Solids Struct. 40 (18) (2003) 4729–4748.
[66] M. Lepidi, Catenary configuration and geometric stiffness matrix of inextensible cables: analytical high-order asymptotic solutions for parametric design, 2023, submitted for publication.
[67] S. Verykokou, C. Ioannidis, An overview on image-based and scanner-based 3d modeling technologies, Sensors 23 (2) (2023) 596.
[68] H.S. Park, H. Lee, H. Adeli, I. Lee, A new approach for health monitoring of structures: terrestrial laser scanning, Comput.-Aided Civ. Infrastruct. Eng. 22 (1) (2007) 19–30.
[69] J. Curt, M. Capaldo, F. Hild, S. Roux, Modal analysis of a wind turbine tower by digital image correlation, J. Phys. Conf. Ser. 1618 (2) (2020) 022002, IOP Publishing.
[70] D. Tan, J. Li, H. Hao, Z. Nie, Target-free vision-based approach for modal identification of a simply-supported bridge, Eng. Struct. 279 (2023) 115586.
[71] C.Z. Dong, F.N. Catbas, A review of computer vision–based structural health monitoring at local and global levels, Struct. Health Monit. 20 (2) (2020) 692–743.
[72] F. Hild, S. Roux, Optical methods for solid mechanics, in: P. Rastogi, E. Hack (Eds.), A Full-Field Approach, Volume 367, Wiley-VCH Weinheim, Germany, 2012, pp. 183–228, chapter Digital Image Correlation.